PREDICTED BEHAVIOUR OF THE AGN 201 REACTOR AT HIGH POWER LEVELS

WILLIAM B. H. COOKE

PREDICTED BEHAVIOUR OF THE AGN 201 REACTOR AT HIGH POWER LEVELS

* * * * *

W. B. H. Cooke

PREDICTED BEHAVIOUR OF THE AGN 201 REACTOR

AT HIGH POWER LEVELS

by

W. B. H. Cooke

Lieutenant, Royal Canadian Navy

Submitted in partial fulfillment of
the requirements for the degree of

MASTER OF SCIENCE
IN
MECHANICAL ENGINEERING

United States Naval Postgraduate School
Monterey, California

1 9 6 1

PREDICTED BEHAVIOUR OF THE AGN 201 REACTOR AT HIGH POWER LEVELS

by

W. B. H. Cooke

This work is accepted as fulfilling
the thesis requirements for the degree of
MASTER OF SCIENCE
IN
MECHANICAL ENGINEERING
from the
United States Naval Postgraduate School

ABSTRACT

In anticipation of the AGN 201 nuclear reactor's operation at a power of 1,000 watts for short periods of time and at 20 watts continuously, a prediction of the behaviour during a rapid power rise is obtained from digital computer solutions of the reactor kinetic equations. The experimental and analytical work which provided the coefficients for the equations is outlined. Solutions of the equations indicate the peak power which may be achieved, the time during which 1,000 watts may be obtained, and the temperature rise that results.

The writer wishes to express his appreciation for the assistance and encouragement given him by his thesis advisor Associate Professor H. E. Handler, and by Associate Professor C. P. Howard and Associate Professor R. M. Thatcher, all of the U. S. Naval Postgraduate School, and for the assistance of the reactor facility personnel in obtaining experimental data.

TABLE OF CONTENTS

LIST OF ILLUSTRATIONS

TABLE OF SYMBOLS

α_o	Thermal coefficient of expansion
α'	Ratio of radiative capture cross section to fission cross section based on measured values
B^2	Buckling
c	Specific heat
C	Concentration of the ith delayed neutron precursor
G_T	Temperature coefficient of reactivity
D	Neutron diffusion coefficient
e	Energy produced per fission
f	Thermal utilization factor
$f_{1+\alpha}$	Ratio of $\frac{1+\alpha' f_{1+\alpha'}}{1+\alpha'}$ where α' is defined above and $f_{1+\alpha'}$ is the f non-$1/v$ factor for the ratio of the thermal group radiative capture to fission cross sections
h_c	Heat transfer contact resistance coefficient
k_∞	Infinite-system multiplication factor
k_{eff}	Effective multiplication factor
k_o	Boltzman's constant
K	Thermal conductivity coefficient
K_o	Thermal conductance
ℓ_r	Characteristic length (e.g. extrapolated radius)
L	Neutron diffusion length
n	Neutron density for a unit volume
N_o	Avogadro's number
p	Resonance escape probability
P_f	Fast non-leakage probability
P_s	Slow non-leakage probability
$\dot{q}_f$	Heat generation rate per unit volume

$\dot{q}_o$	Maximum heat generation rate per unit volume
Q	Total heat generation rate
r	Radius or position vector
R_e	Extrapolated radius
S	Source of neutrons per unit volume per second
T	Temperature
ΔT	Difference between mean temperature of core and ambient temperature
t	Time
u	Lethargy
V	Volume
β	Fraction of delayed neutrons per neutron emitted in fission
γ	Delayed neutron effectiveness
ξ	Average logarithmic energy decrement per collision
η	Number of fast neutrons due to thermal fissions emitted per thermal neutron absorbed in fuel
Λ	Neutron lifetime
λ	Decay constant
$\bar{\mu}_o$	Averaged cosine of scattering angle
ν	Number of neutrons emitted per fission
ρ	Reactivity
ρ_o	Mass density
Σ	Macroscopic neutron cross section
σ	Microscopic neutron cross section
$\hat{\sigma}$	Westcott's average neutron cross section
τ	Reactor period
v	Neutron velocity

ϕ	Total neutron flux
ε	Fast fission factor
τ	Fermi Age
Σ	Summation sign

Subscripts

Cross sections	a	absorption
	f	fission
	r	removal
	c	capture
	es	elastic scattering
	t	total
Two-Group equations	f	fast neutron group
	s	slow neutron group
Two-Group Two-Region equations	1	fast neutron group incore
	2	slow neutron group in core
	3	fast neutron group in reflector
	4	slow neutron group in reflector
	c	core
	r	reflector
Core Materials	F	fuel
	0	materials other than fuel
Temperature	i	inside surface for shell
	0	center for solid body
	o	outside surface for shell
	1	outside radius for solid body

Some information presented in this investigation is proprietary to Aerojet General Nucleonics, a California Corporation, and is not to be reproduced, used, or reduced to practice without a prior written agreement with Aerojet General Nucleonics.

1. Introduction.

The AGN 201 nuclear reactor is a low power reactor designed for educational uses. Usually, it is licensed to operate at 100 milliwatts and serves to demonstrate many of the basic characteristics of reactors. Also, at this power, the peak neutron flux of about 4.5×10^6 neutrons/cm^2-sec is sufficient for the creation of many radioactive isotopes in practical quantities.

For other isotopes, however, it is desirable or necessary to have a much higher neutron flux and it has been proposed that the AGN 201 be operated for short periods at a power of 1,000 watts. Several of these reactors have been operated at somewhat higher powers, but none have operated as high as 1,000 watts. The limiting factor on elevated power operation is the lack of a cooling system. With no means of increasing the rate of heat transfer from the core, the overall core temperature increases. Since the reactor has a negative temperature coefficient of reactivity, a rise in temperature reduces the available excess reactivity, and the rate at which power may be further increased is reduced.

The maximum steady-state power is that power at which the rate of heat generation in the core is equal to the rate of heat transfer from the core and the corresponding overall temperature of the core has reduced the initial excess reactivity to zero. For the AGN 201, maximum steady-state power has been estimated to be approximately 20 watts. High powers, such as 1,000 watts, would be achieved during the transient period following a relatively large increase in reactivity if the reactor core is initially at room temperature. Under such conditions, power

can be increased rapidly by several orders of magnitude before the temperature has risen sufficiently to make the reactor sub-critical.

The transient behaviour of a reactor can be predicted using reactor kinetic equations based on various approximations. In general, the equations cannot be solved analytically due to the coupling between them, and analog computer solutions are frequently obtained for cases where variations of the dependent variables are not large. When the dependent variables change by orders of magnitude, numerical methods may be applied to solve the equations using a digital computer.

It is the purpose of this investigation to establish a set of reactor kinetic equations for the AGN 201 and obtain a solution to the equations using a digital computer for the case of a rapid rise in power. Features of significance to be obtained from the solution include an estimate of the peak power that may be achieved (or in the runaway accident sense, a peak power which will not be exceeded), the length of time that a power of 1,000 watts may be maintained, and the temperatures which would result. The latter is significant since there is a thermal fuse in the core which allows the bottom half of the core to drop away in the event of overheating. The fuse is always at a higher temperature than the rest of the core.

The coefficients of the kinetic equations are obtained from experimental data or from calculations. The available excess reactivity of the reactor, the rate at which reactivity can be added, and an estimate of the temperature coefficient of reactivity can be obtained experimentally. The remaining nuclear coefficients and heat transfer coefficients must be calculated from the tabulated data for materials and compared where

possible with known physical characteristics of the reactor to establish their reliability. For example, the nuclear parameters should predict the actual critical mass, and the calculated kinetic equation coefficients, when applied to a computer solution for low power transient behaviour, should provide curves in reasonable agreement with curves obtained experimentally.

The dependent variables in the kinetic equations are temperature, neutron density, and the concentrations of the six delayed neutron precursors. The effect of nuclear poisons is omitted since the peak flux at 1,000 watts is in the order of 10^{11} neutrons/cm^2-sec at which poison effects are not significant. From neutron density, neutron flux and power can be determined. In the following sections, a description of the reactor, the procedure for obtaining parameters, and the method of obtaining computer solutions for neutron density and temperature are described.

2. Description of the Reactor

The reactor assembly is shown in Figure 1 and further detail of the core is shown in Figure 2. The core material is a homogeneous mixture of polyethylene and uranium dioxide; the uranium is 20 percent enriched in Uranium 235. The core is surrounded by a high-density graphite reflector, a lead shield, and a water shield. For powers higher than 100 milliwatts additional shielding is added in the form of concrete blocks. The structural material in the core region is 6061-T6 aluminum.

Control is affected by the insertion and withdrawal of rods containing essentially the same material as the core. Three rods are the same size; two of these serve as safety rods, and the third is a coarse control rod. The fourth rod, which is smaller, provides fine control.

Table 1 summarizes the characteristics of the AGN 201 series of reactors in general.

Table 1 AGN Characteristics

Power, licensed	100 mw
Peak thermal flux	4.5×10^{6} n/cm^{2}-sec
Critical mass	665/gm of U^{235} (20% enriched UO2)
Core size	25 cm. diameter, 24 cm high
Moderator	11 kgm polyethylene
Impregnation density	55 mg U^{235} /cm^{3}
Reflector (graphite)	20 cm thick (density 1.75 gm/cm^{3})
Shield (lead)	10 cm thick
Shield (water)	55 cm thick
Maximum Excess reactivity	$\sim$0.2% @ 20°C (glory hole empty)
	$\sim$0.4% @ 20°C (polyethylene in glory hole)
Temperature Coefficient of Reactivity	$\sim -3 \times 10^{-4}$/°C

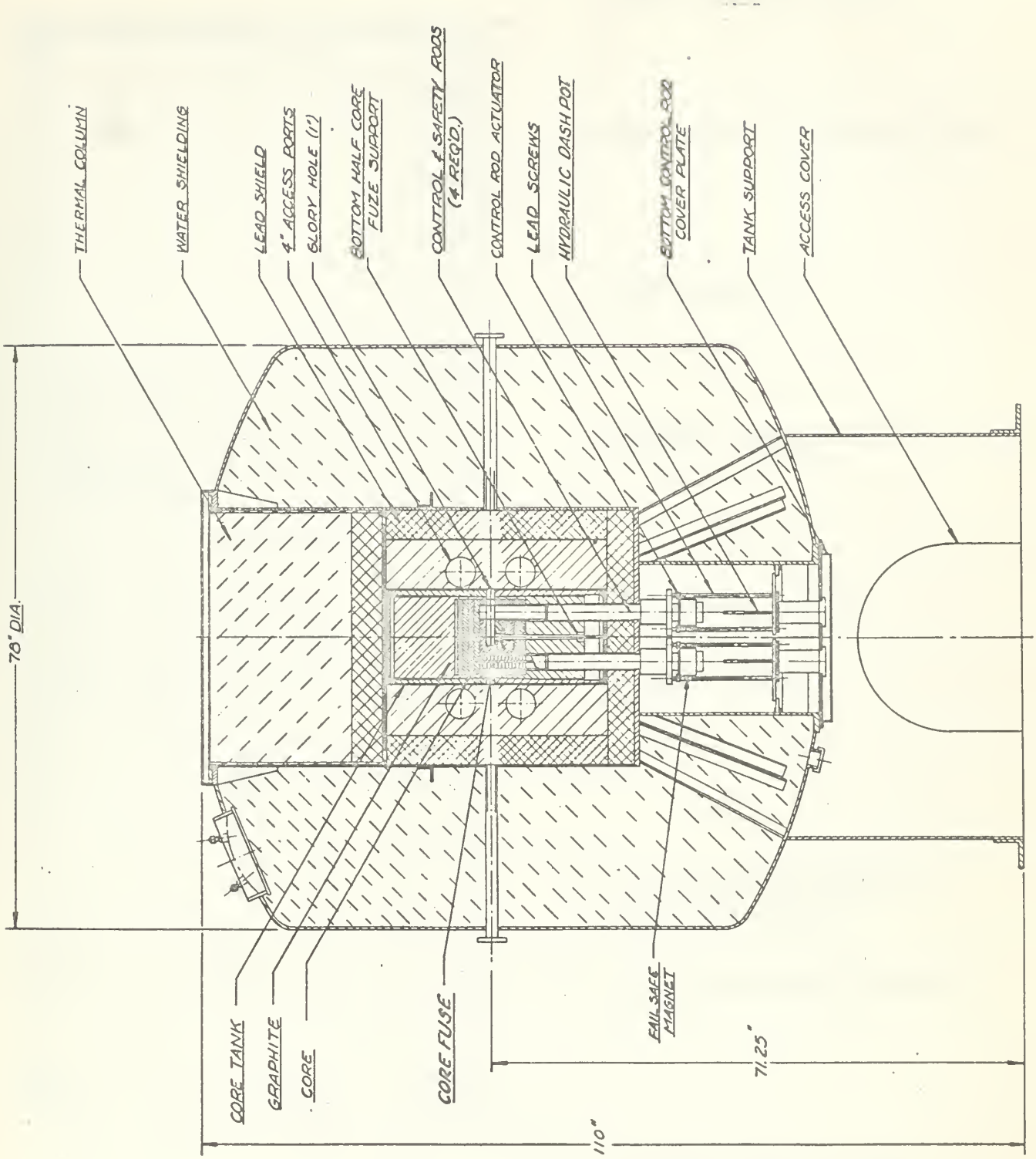

Figure 1. AGN 201 Reactor Assembly

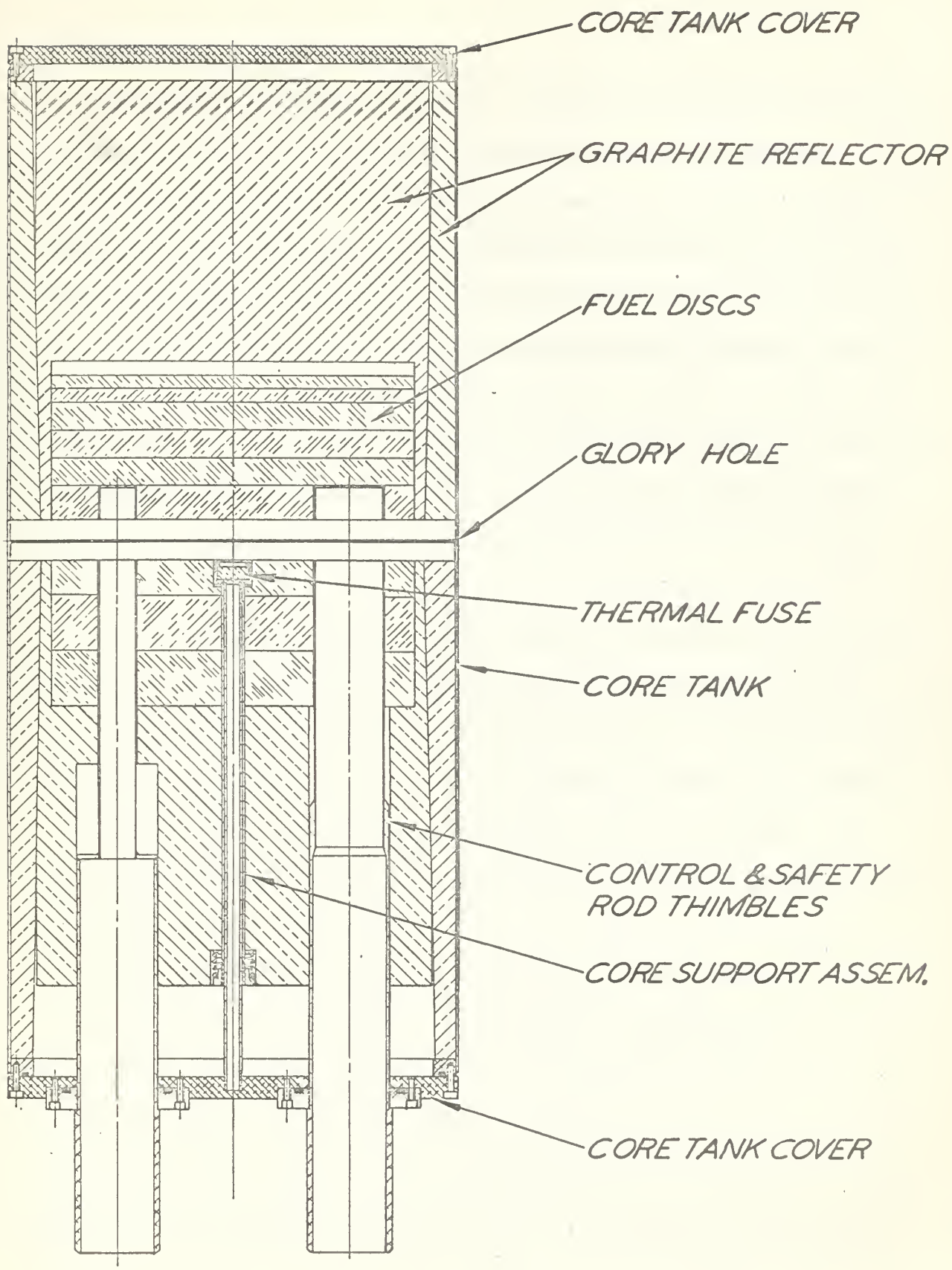

Figure 2. AGN 201 Core Assembly

3. Preliminary Considerations.

From the characteristics noted in the previous section, it is evident that the reactor has little excess reactivity at room temperature. During laboratory periods, it has been found that five or six of the small cadmium covers used around foils in thermal flux determinations are sufficient to shut the reactor down. This limited excess reactivity and the strong negative temperature coefficient would prevent continuous operation with the glory hole empty at core temperatures above 27°C. Since the reactor has no cooling system, the average temperature in the core would increase seven degrees quite rapidly when the reactor is operating with a high neutron flux and the resulting high heat generation rate in the core.

One would expect then that it is necessary to approach high powers as rapidly as possible, that temperature would increase significantly with a corresponding reduction in reactivity when the reactor is at sufficiently elevated powers, and that in a relatively short time a negative reactivity would result causing a decrease in power. Subsequent long period oscillations of power about an equilibrium position probably would be the end result.

To establish a set of equations which predict this behaviour and can be solved, it is necessary to use a number of approximations. Foremost of these is the Diffusion Equation approximation of the exact Boltzman Equation; in this approximation isotropy of the neutron velocities is assumed. Also, exact energy distributions are replaced by the appropriate averages over energy intervals. Dividing the neutron population into groups according to the energy provides excellent results if

a large number of groups are established. The complexity of solving this problem, however, is not justified except in the most refined determinations of neutron behaviour in materials.

One-group theory, modified one-group theory, Fermi Age theory and two-group theory are frequently used as approximations. Of these, Fermi Age theory is a good approximation for reactors moderated by relatively heavy materials, while two-group theory provides reasonable results for reactors in which hydrogen is the principal moderating material. (1) When the moderator contains hydrogen and a number of heavier materials, the Selengut - Goertzel equation yields better results than a two-group approach since the Selengut - Goertzel equation treats hydrogen slowing down and slowing down due to other materials separately. However, to obtain reasonable parameters for the time dependent problem with more than one region, two-group theory is more readily applied.

A second area of approximations is the geometric model of the reactor to be assumed. Since the theories require the solution of several simultaneous partial differential equations containing the Laplacian and two or three independent variables, a solution for the actual geometry would be extremely difficult to obtain. The problem is sufficiently complicated if one assumes a core region surrounded by a reflector region with cylindrical geometry, and ignores all details of structural materials and construction. This model is satisfactory from the nuclear standpoint, but further consideration is required in connection with heat transfer, since the structural aluminum is a good conductor and the boundary and interface conditions have a different physical significance. These features are discussed in Section 6.

For a single region containing one material, the time-dependent neutron diffusion equation for a single energy group simplifies to:

$$D\nabla^2\phi(\vec{r},t) - \Sigma\phi(\vec{r},t) + S(\vec{r},t) = \frac{\partial n(\vec{r},t)}{\partial t}$$

and for this same region the time-dependent heat diffusion equation is given as:

$$K\nabla^2 T(\vec{r},t) + \dot{q}_f(\vec{r},t) = \rho_o c \frac{\partial T(\vec{r},t)}{\partial t}$$

In both equations, the coefficients may be functions of the independent variables in the two equations; for example, the conductivity and diffusion coefficient are both temperature dependent. The source term in the heat diffusion equation is proportional to the thermal neutron flux for the same point in the region, and, in turn, the source term and the coefficients of the neutron diffusion equation are affected by the temperature.

Considering a small volume element in the region using a two-group approach, we have the following coupled partial differential equations:

$$D_f\nabla^2\phi_f - \Sigma_r\phi_f + \nu\Sigma_f\phi_s(1-\beta) + \sum \lambda_i C_i = \frac{\partial n_f}{\partial t} \quad (i = 1 \text{ to } 6)$$

$$D_s\nabla^2\phi_s - \Sigma_a\phi_s + \bar{P}\Sigma_r\phi_f = \frac{\partial n_s}{\partial t}$$

$$\nu\Sigma_f\phi_s\beta_i - \lambda_i C_i = \frac{\partial C_i}{\partial t}$$

$$K\nabla^2 T + E\phi_s = \rho_o c \frac{\partial T}{\partial t}$$

where the subscripts "f" and "s" refer to the fast and slow neutron groups, respectively, and where E is a factor to convert neutron flux in the element to the corresponding heat generation rate. These equations could be solved by numerical methods using finite difference techniques and a mesh system. The complexity of such a solution and

the time required to solve this problem are prohibitive even with the use of a high speed digital computer. Further discussion of this problem is included in Section 8.

A more practical approach, and the approach used most frequently, is to obtain from the above equations a set of ordinary differential equations amenable to computer solutions. Considering only the thermal group of neutrons, the diffusion equation may be written:

$$D\nabla^2\phi - \Sigma_a\phi + \nu\Sigma_f(1-\beta)pP_f\phi + p'P_f'\sum\lambda_i C_i = \frac{\partial n}{\partial t}$$

where $p'P_f'$ refers to the resonance escape probability and the fast non-leakage probability of the delayed neutrons. With the assumption that the flux can be calculated from the wave equation

$$\nabla^2\phi(\vec{r},t) + B^2\phi(\vec{r},t) = 0$$

the equation above may be reduced to

$$\frac{dn}{dt} = \frac{k_{eff}}{\Lambda}(\rho-\beta)n + \frac{p'P_f'}{k_{eff}}\sum\lambda_i C_i$$

(See Appendix 1)

This equation coupled with the six ordinary differential equations for the delayed neutron precursors and a differential equation for temperature can be solved readily by numerical methods.

Irrespective of the approach, it is necessary to obtain values for coefficients and parameters which are required for the equations. Some of these parameters can be calculated quite accurately, and some data are tabulated. In other cases, the values must be estimated. The test of any set of parameters selected is that they predict features of the reactor which are known. For example, the parameters should, when used

in the appropriate equations, yield approximately the known critical mass and the steady-state flux distribution, and solutions of the transient equations at low power should agree with corresponding curves from the reactor. For this reason a number of experiments were carried out on the reactor to obtain data both to supplement calculated data and to provide verification of calculated data. These experiments are described in the following section.

4. Experimental Data Obtained.

(a) Excess Reactivity Available

One of the most important parameters required for the high power estimation is the maximum excess reactivity available. Since this quantity is very small, it cannot be calculated with any degree of accuracy but may be determined experimentally with reasonable precision from the reactor period. The rate at which excess reactivity can be added is also of importance. Two forms of reactivity can be accomplished, the step input and the ramp input. The ramp input is the usual form of input, but a step input could be arranged if necessary.

The method of applying a ramp input would be the insertion of a rod, and, since the coarse rod contributes more reactivity per unit length than the fine rod, coarse rod movement only is considered. The procedure then for determination of excess reactivity and rate of application of excess reactivity was as follows:

With the fine rod fully inserted and the glory hole empty, the reactor period was determined for various positions of the coarse rod from the Varian Recorder charts.[1] This experiment was repeated with polyethylene in the glory hole. Finally, the actual rate of coarse rod travel was established from the average of a number of runs in which travel for a specified stop watch time was measured. The temperature of the water

[1] Two ion chambers and one BF_3 counter are fitted in the reactor for monitoring the power level.[3] A Varian Recorder is used to record the micro-micro ammeter output for either ion chamber or the count-rate meter of the BF_3 counter.

shield on the day of the experiment was (21.2 ± 0.5)°C and it is assumed that the core temperature was very nearly the same.

The rate of coarse rod movement was found to be (26.3 ± 0.2) cm/min.; this figure coupled with an almost linear relation between insertion and excess reactivity provided data for a ramp input. The relation between rod insertion and $\frac{\rho}{\gamma}$, the ratio of reactivity to delayed neutron effectiveness, is shown in Figure 3(b). It is noted that the contribution to reactivity per unit length of the rod is the same for polyethylene in the glory hole as for an empty glory hole for practical purposes. The linear relationship agrees with the approximately linear portion of the standard S-curve since the rods of the AGN 201 do not pass through the entire core. From the slope of the curve in Figure 3(b), the value of $\frac{\rho}{\gamma}$ per unit length is approximately 5.61×10^{-4}/cm.

The function of excess reactivity originates from the equation

$$\rho = \frac{\Lambda}{k_{eff} T} + \sum \frac{\gamma_i \beta_i}{1 + \lambda_i T}$$

$$\approx \frac{\Lambda}{k_{eff} T} + \gamma \sum \frac{\beta_i}{1 + \lambda_i T}$$

The factor γ allows for higher effectiveness of the delayed neutrons as compared to the prompt fission neutrons in reaching thermal energy. In the experiments for excess reactivity, the periods used were sufficiently long so that the first term of the equation was insignificant. Since the factor γ is not well known, $\frac{\rho}{\gamma}$ was computed and can be used in this form as shown in Section 7. Further discussion of the origin and significance of the equation is given in Appendix 1.

Since the worth per unit length of the coarse rod is approximately constant over the last few centimeters of travel, the worth of the

polyethylene in the glory hole can be related to a length of coarse rod. Over a period of time, the coarse rod position with and without polyethylene in the glory hole was noted in connection with the temperature coefficient estimation. The difference of positions, the worth of the polyethylene is 3.94 $\pm$ .03 cm.

(b) Temperature Coefficient of Reactivity.

The temperature coefficient experiment was actually a rough attempt to check the reported experimental value of $(-2.75 \times 10^{-4})/°C$.[1] This experiment assumes that the effect on the core of a constant temperature throughout is the same as for the numerically equal average temperature of a temperature distribution in the core. This is not quite accurate because a volume element near the centre of the core has a greater "importance" than a volume element near the surface of the core and is at a higher temperature. If an average temperature is used, it should be weighted according to the importance distribution. The experiment then serves only to provide an approximation of the magnitude of the temperature coefficient of reactivity.

Over a period of several weeks, the overall temperature of the reactor was raised and lowered over as wide a range as possible by adjusting the thermostat of the heating system in the reactor facility. The temperature range achieved was only two and a half degrees by this elementary procedure, but sufficient difference was noted in the position of the coarse rod for criticality to make the plot shown in Figure 3(a).

[1] AGN Report #22, Aerojet General Nucleonics.

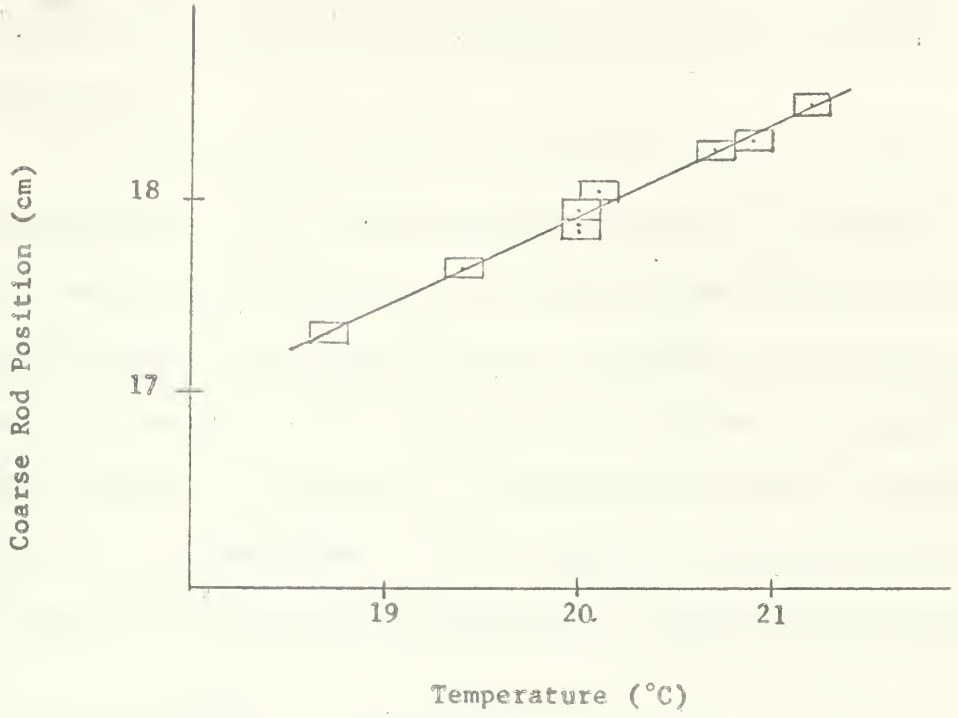

Figure 3(a) Temperature Coefficient of Reactivity Determination

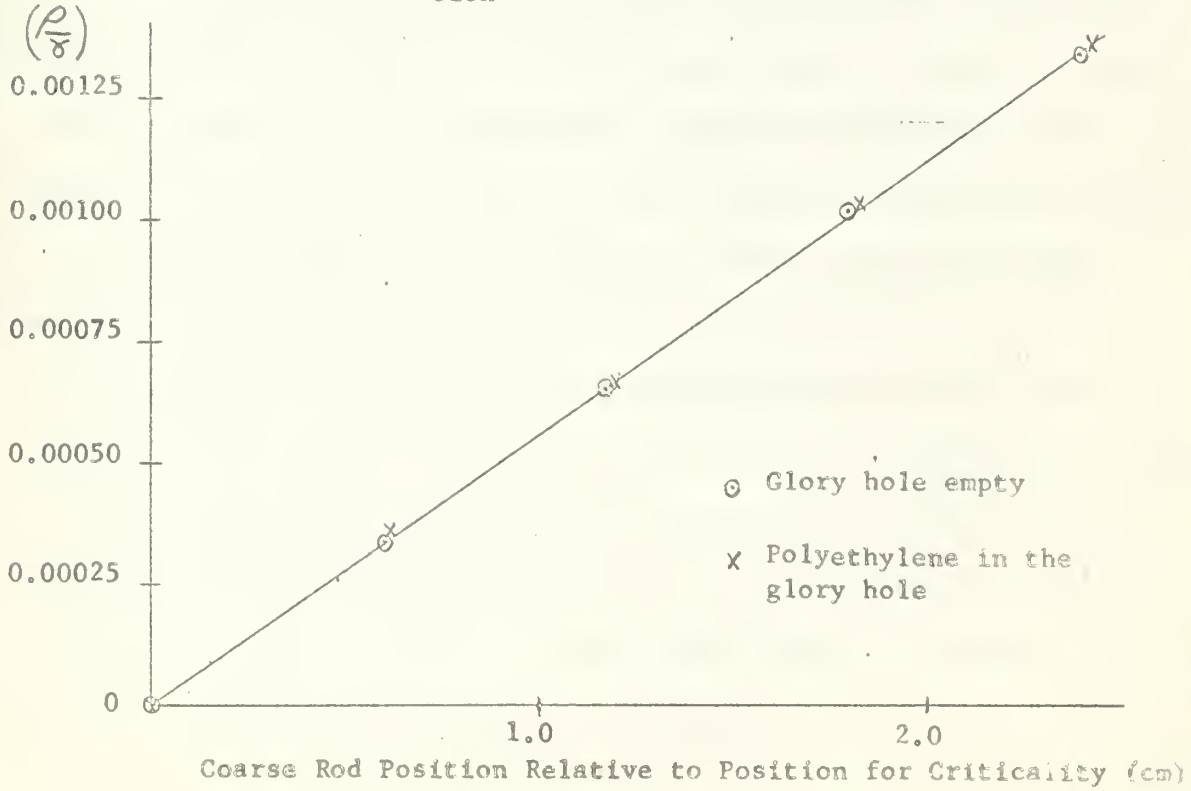

Figure 3(b) Excess Reactivity as a Function of Coarse Rod Position

The least square curve through the points has a slope of + .472 cm/°C corresponding to a reactivity of - 2.75 x 10^{-4}/°C. This agrees surprisingly well with the value obtained by AGN for a much wider range of temperatures.

At this point, the questions may be raised as to whether the worth per centimeter of the coarse rod determined at 21.2°C is the same for other temperatures around 20°C and if the polyethylene has an effect on the temperature coefficient estimate as compared to the reactor with the glory hole empty. A rerun of the excess reactivity experiment at a different temperature produced no significantly different results and the worth of the polyethylene over the temperature range showed no consistent tendency to increase or decrease as a function of temperature.

(c) Drop Test

A further experiment providing some insight to the worth of the polyethylene in the glory hole was carried out; the primary purpose of this experiment was to approximate a negative step input so that the computer programs could be checked. This experiment consisted of obtaining a Varian Recorder chart of the reactor behaviour when the polyethylene was pulled suddenly from the glory hole while the reactor was at a steady power. This procedure is similar to the Drop Test method of obtaining reactivity for a group of rods (1) (4). Plotting the logarithum of flux versus time over the first few seconds and extrapolating back from the approximate straight line slope as shown in Figure 4 provides a value of flux ϕ_1, on the t = 0 axis. Then from the equation

$$\frac{\phi_0}{\phi_1} = 1 + \frac{\delta k_{eff}}{\sum \delta_i \beta_i}$$

$$\approx 1 + \frac{\rho/\alpha}{\sum \beta_i} k_{eff}$$

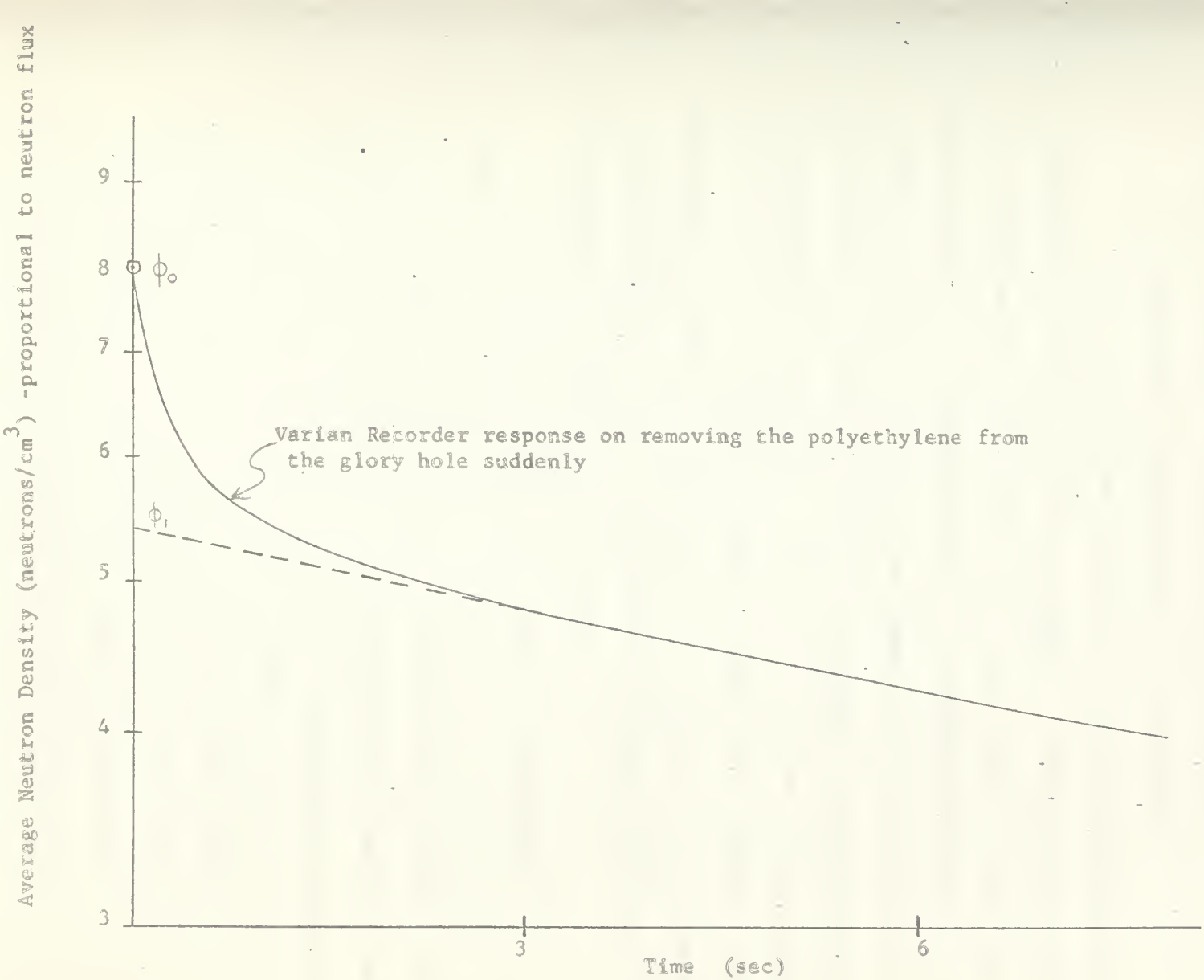

Figure 4 Drop Test Simulation

a value for $\frac{\rho}{\delta}$ of 0.0023 $\pm$ 0.0002 is obtained which agrees with the value 0.0022 obtained from the product of coarse rod worth per centimeter and worth of polyethylene in centimeters of coarse rod.

(d) Neutron Flux Traverse through the Glory Hole

The relative thermal neutron flux and the epi-cadmium flux through the glory hole are shown in Figure 5. The fluxes were obtained by irradiating bare and cadmium-covered indium foils at various equi-spaced positions in the glory hole and determining the activity of the radiated foils with a scintillation counter. The flux plots were considered necessary to obtain an indication of geometric buckling by measuring the extrapolated core radius. Also, from the slopes at the interface and the curvature in each region, relative values of the diffusion coefficients and values of diffusion lengths could be estimated. The experimental precision of these flux plots is not particularly good, but the plots serve the purposes for which they were intended.

It is of interest to note that there is a significant dip in the thermal flux at the centre of the core due to the thermal fuse so that the peak thermal flux is about one centimeter from the center. Also, the functions associated with the minor buckling of a two-group analysis which are usually positive for thermal flux and negative for fast flux at the core-reflector interface are of reversed sign for the AGN 201. This fact was useful as a guide to obtaining relative values of diffusion coefficients and flux equation terms in the parameter determinations discussed in the next section. One further use made of the flux plot was a location of the center of the core; first attempts at obtaining a flux plot indicated that the foil holders in use were off by about

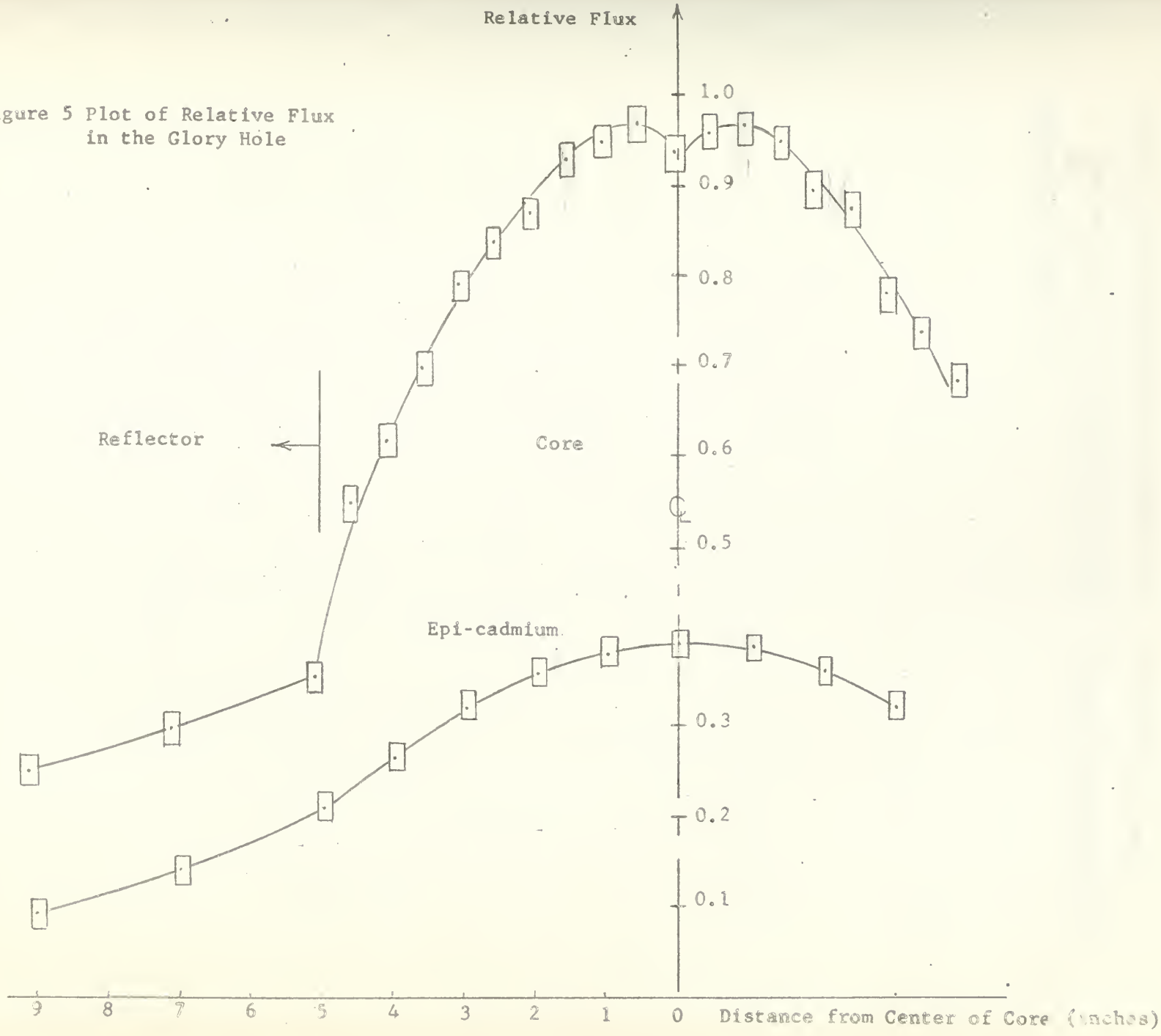

Figure 5 Plot of Relative Flux in the Glory Hole

one-half inch in calibration and subsequent corrections were made.

The data of this section and the data of the next two sections are summarized on page 49 .

5. Theoretical Nuclear Parameters.

As was mentioned previously in Section 3, two-group theory provides a reasonable approximation for reactors moderated by hydrogenous materials. If a set of two-group parameters are obtained which predict quite accurately several known features of the reactor, it is assumed that these parameters and other data calculated from them are good approximations for subsequent computations.

Two-group theory for a reactor with a single reflector region provides the following diffusion equations assuming no spatial dependence of coefficients within each region:

Core

$$D_1 \nabla^2 \phi_1(\vec{r}) - \Sigma_r^{(1)} \phi_1(\vec{r}) + \nu \Sigma_f \phi_2(\vec{r}) = 0$$

$$D_2 \nabla^2 \phi_2(\vec{r}) - \Sigma_a^{(2)} \phi_2(\vec{r}) + P_c \Sigma_r^{(1)} \phi_1(\vec{r}) = 0$$

Reflector

$$D_3 \nabla^2 \phi_3(\vec{r}) - \Sigma_r^{(3)} \phi_3(\vec{r}) = 0$$

$$D_4 \nabla^2 \phi_4(\vec{r}) - \Sigma_a^{(4)} \phi_4(\vec{r}) + P_r \Sigma_r^{(3)} \phi_3(\vec{r}) = 0$$

The solutions of these equations provide equations for the steady-state slow and fast flux at all points in the core and reflector and a criticality determinant from which the critical mass can be calculated.

(a) Reflector Parameters

For the reflector, five parameters are required: the thermal and fast diffusion coefficients, the macroscopic thermal cross section, the resonance escape probability and the fast neutron removal cross section. The removal cross section is obtained from the ratio of the fast diffusion coefficient over the ficticious fast diffusion length (frequently taken as equal to the Fermi Age).

The reflector of the AGN 201 is manufactured from high-density reactor-grade graphite with a nominal density of 1.75 gm/cm^3. A rough check on the density of a sample yielded 1.74 $\pm$ .02 gm/cm^3 so that the nominal figure is satisfactory for calculations. The standard density for graphite in most references is 1.60 gm/cm^3 and the tabulated nuclear parameters for commerical graphite are based on this density (1). Applying a correction to the tabulated parameters for density difference, the following data are obtained:

$$D_4 = 0.838 \text{ cm.}$$
$$\Sigma_a^{(4)} = 0.000374 \text{ cm}^{-1}$$
$$D_3 = 0.929 \text{ cm}$$
$$\mathcal{T} = 304 \text{ cm}^2$$

Then $$\Sigma_r^{(3)} = \frac{D_3}{\mathcal{T}} = 0.00306 \text{ cm}^{-1}$$

The remaining factor, the resonance escape probability p_r, is effectively 1.00 since carbon has no resonance peaks in the epithermal range (5) and the impurity content of reactor-grade graphite is very low.

(b) Core Parameters - First estimate

Unfortunately, core parameters are not as readily obtained. Polyethylene has been used quite frequently in shielding and as the moderator of critical assemblies, but, for the most part, the nuclear data for water have been used in calculations (with a hydrogen atom density ratio correction). Very little experimental nuclear data on polyethylene itself are available.

From the official records of "License Material" at the U. S. Naval Postgraduate School, the following data pertain to the core:

Total weight of U^{235} 665.03 gm

Percent U^{235} in uranium	19.93%
U^{235} density in polyethylene	0.055 gm/cm^3
Total weight of components	14781.6 gm
Total weight of Uranium	3337.67 gms

The uranium is in the form of uranium dioxide particles compacted with the polyethylene.

The value of 665.0 gms for the weight of U^{235} is probably quite accurate, and for all components, except the thermal fuse, the weight ratio of U^{235} to total weight is consistent (0.0450 ± 0.0003). If the impregnation density is 0.055 gm U^{235} cc., the overall density is 1.22 gm/cc. From the weight of components and the volume calculated from AGN 201 blueprints, a density of (1.22 ± 0.01) gm/cc. is indicated for core discs but a slightly lower value is obtained for rod components. Since the rods form but a small part of the core and the error involved is less than one percent, an overall density of 1.22 gms/cc. will be assumed for the polyethylene and uranium dioxide.

The core also contains about 250 cm^3 of aluminum, and about 50 cm^3 of pure polyethylene will be in the glory hole to obtain maximum excess reactivity. The aluminum has little effect on overall nuclear characteristics of the core since both the absorption cross section and scattering cross section of aluminum are relatively small. The polyethylene contributes significantly to the excess reactivity as previously noted, but the volume concerned is about 0.4% of the core volume. The calculations of the core characteristics can then be based with little error on the uranium-impregnated polyethylene with a density of 1.22 gm/cc. On this basis the Table 2 data are calculated. Since the volume ratio of UO_2 to the polyethylene moderator is small, the fast and thermal diffusion coefficients

Table 2

Core Material Data

Weight of U^{235}	665.03 gm
Core material volume	12,100 cm^3
Overall density of core	1.22 gm/cc
Densities U^{235}	0.055 gm/cc
U^{238}	0.221 gm/cc
Uranium	0.276 gm/cc
Oxygen	0.037 gm/cc
UO_2	0.313 gm/cc
Carbon	0.779 gm/cc
Hydrogen	0.130 gm/cc
Polyethylene	0.909 gm/cc
Volume ratio of UO_2 to total volume 2.9%	

and the Fermi Age are approximately the same as for pure polyethylene.

Three sources of neutron cross sections are included in the Bibliography and are referenced in Table 3 below. Although the 1960 Supplement to BNL 325 is not included, data from the supplement were used in reference (7). All microscopic cross sections are in barns.

For U^{235}, Westcott's tables (6) will be used since they provide the most up to date data on materials with non - $\frac{1}{v}$ cross sections and allow for the 1/E tail of the neutron distribution.

Using the densities of the individual materials and the cross sections

as listed, microscopic absorption cross sections averaged over a Maxwellian distribution for a temperature of 20°C are obtained from the equation

$$\overline{\Sigma} = \frac{1}{1.128}\left(\frac{\sigma_i N_o \rho_{oi}}{W_i}\right) = \sum \overline{\Sigma}_i$$

Table 3

Neutron Cross sections

	σ_a	σ_s	σ_f	η	ν
H (gas	.332(5) (7)	38(5) (7)			
C	.0034(5)	4.2(5) (7)			
	.00373(7)				
O	.0002(5)	4.2(5) (7)			
	.0002(7)				
U^{235}	694(5)	10(5)	582(5)	2.07(5)	2.47(5)
	694(7)	10(7)	582(7)		
	683.04(6)		577.01(6)	2.0695(6)	2.4498(6)[1]
U^{238}	2.71(5)(6)(7)		.0005(7)		

The cross sections for U^{235} in the above equation are obtained from Westcott's tables as

[1] Westcott's values are those to which tabulated cross sections were normalized and differ slightly from accepted values.

$\hat{\sigma}_f$ = 562.5 barns [1]

$\hat{\sigma}_a$ = 669.2 barns

for r = 0.03 and the S_2 cut - off. The value of r defines the proportion of epithermal neutrons in the spectrum; whereas this was not measured experimentally for the AGN 201, the value is considered to be a reasonable estimate. The S_2 cut - off corresponding to cutting off the neutron spectrum above 4.95 KT, is recommended in Westcott's tables for general cases.

Then $\bar{\Sigma}_a^{235} = 0.0837 \text{ cm}^{-1}$

$\bar{\Sigma}_f^{235} = 0.0710 \text{ cm}^{-1}$

and $\bar{\Sigma}_a = 0.0231 \text{ cm}^{-1}$ for the oxygen, carbon and hydrogen lumped together.

With these cross sections the product of the thermal utilization and the fast neutrons produced by thermal fission per thermal absorption in the fuel can be obtained as

$$\eta f = 1.594$$

From the equation (1)

$$\varepsilon - 1 = \frac{\frac{\Sigma_t^8}{\bar{\Sigma}_t}\left(\nu - 1 - \frac{\sigma_c^8}{\sigma_f^8}\right)\frac{\sigma_f^8}{\sigma_t^8}}{1 - \left(\nu\frac{\sigma_f^8}{\sigma_t^8} + \frac{\sigma_{es}^8}{\sigma_t^8}\right)\frac{\Sigma_t^8}{\bar{\Sigma}_t}}$$

[1] Four figure accuracy is not justified but data of the tables maintain the additional figures.

and values tabulated with the equation, an approximation can be obtained of the fast fission factor for the AGN 201. As expected ε does not differ significantly from 1.000. Finally, with the calculation of the resonance escape probability "p" using epithermal scattering cross sections and Figure 14 of Section 6 - 2 in Reference (1), a value of "k_∞" can be obtained for the core material.

$$p_c = 0.960$$

$$k_\infty = \eta f \varepsilon p_c = 1.530$$

The fast diffusion coefficient for the core material as a function of lethargy may be approximated using the equation

$$D_1(u) = \frac{1}{3 \sum \Sigma_{s_i}(u)(1-\bar{\mu}_o)_i}$$

where "i" refers to the nuclide. Since Σ_{s_i} varies with lethargy, a numerical integration was carried out using BNL 325 curves and equal lethargy intervals. The contribution of oxygen and uranium scattering was neglected since the macroscopic scattering cross sections of these materials are relatively small. The numerical integration yielded a value of 0.623 cm for D_1.

To determine the removal cross section $\Sigma_r^{(1)}$, the effective "fast diffusion length" is first obtained. For hydrogenous materials, the so-called Fermi Age is approximately equal to the square of the "fast diffusion length" (2). An experimental value for the Fermi Age of polyethylene has not been published but the Age of polyethylene can be calculated from that of water because the hydrogen of both accounts for most of the macroscopic scattering cross section and the scattering cross section of carbon and of oxygen are similar in the epithermal region.

The principal difference between polyethylene and water is the atomic density. The Fermi Age of a material varies inversely as the product of its density and its averaged microscopic scattering cross section. Roughly then

$$\tau \propto \frac{1}{\rho \Sigma_s^2}$$

and since

τ = 27.7 cm^2 for water (2)

ρ = 0.920 for water

ρ = 0.908 for polyethylene

Σ_s = 1.50 cm^{-1} for water

Σ_s = 1.78 cm^{-1} for the core material

then τ = 19.8 cm^2 for polyethylene

The removal cross section is given by

$$\Sigma_r^{(1)} = \frac{D_1}{\tau} = 0.0237 \text{ cm}^{-1}$$

For the thermal diffusion coefficient, it is necessary to estimate again from the known data for water. The thermal diffusion coefficient for water averaged over a thermal distribution is given as 0.159 cm. Correcting for the ratio of atomic densities provides a first estimate of 0.136 cm. for polyethylene if the scattering cross section and the average cosine of the scattering angles are assumed similar. However, the scattering cross section of polyethylene is as much as 15% higher than that of water at thermal energies and exhibits more strongly the effects of molecular binding. If the discrepency was averaged over a thermal distribution covering the entire thermal range, the difference might be in the order of 10% resulting in an estimate of 0.123 cm for D_2. As a check on this supposition, the relation

$$3D = \frac{1}{\Sigma_t (1-\bar{\mu}_o)}$$

was averaged numerically over a Maxwellian distribution with kT equal to 0.0253 ev. Linear relations were assumed for $(1-\bar{\mu}_o)$ of water and polyethylene and Σ_t as a function of energy was taken from BNL 325 in the case of water and from an unpublished KAPL Paper for polyethylene.[1] The ratio of the two averaged functions when applied to the diffusion coefficient of water (0.159 cm) yielded a corresponding value for polyethylene of 0.125 cm. This value is assumed as a reasonable estimate for purposes of a two-group analysis.

(c) Checking Parameters in Critical Mass Calculations.

With the nuclear parameters calculated thus far in this section, a two-group two-region analysis for cylindrical geometry was attempted for purposes of computing the critical mass as one check on the validity of the parameters. The results of the attempt were unsatisfactory, and subsequent attempts were made with small variations in the parameters in an effort to establish whether the poor results were due to minor inaccuracies within the tolerances of the basic data.

The two-group analysis provides a four-by-four determinant, the terms of which consist of functions dependent on the geometry and on the coefficients of the partial differential equations. This determinant can be expanded into an equation with the most sensitive function of core parameters on one side of the equation and the less sensitive functions on the other side (2).

[1] Private communication with R. E. Slovacek, Knolls Atomic Power Laboratory.

Making slight adjustments to various parameters of the core in either the determinant or the equation to achieve a balance is very laborious and tends to obscure the significance of changes. The matrix formulation of Reference (1) however separates out the parameters of the reflector, which are fairly well known, into a reflector matrix, and the adjustment of parameters in the core matrix is both easier and more enlightening.

When satisfactory results were still not achieved, the analysis was repeated for spherical geometry to establish whether the "corners" omitted in the cylindrical geometry were the source of error. These corners are shown in Figure 6(a). The cases shown in Figure 6(b) and Figure 6(c) can be solved analytically and the case in Figure 6(d) can be approached by iteration using the geometries of 6(b) and 6(c) alternately. However, with a small cylindrical core surrounded by a relatively thick reflector, the corners omitted in 6(d) are significant. The actual core dimensions are very close to the optimum case for cylindrical geometry, and this in turn has very similar characteristics to a sphere. If an equivalent spherical geometry is assumed with the same buckling as the cylinder and approximately the same reflector savings, the omission of a large part of the reflector in the cylindrical geometry case can be avoided.

However, it was found that no justifiable adjustment of the estimated parameters would satisfy the criticality condition. The parameters in every case led to a core size considerably smaller than the actual core.

(d) Effect of Spectrum Hardening

A factor which had not been included in the calculations (and

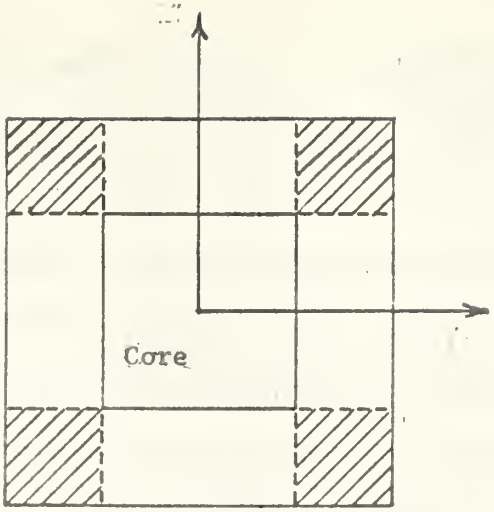

Figure 6(a)

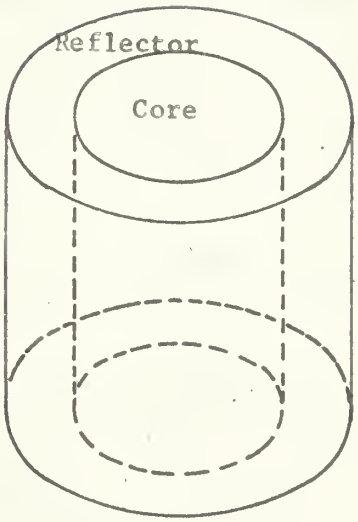

Figure 6(b)

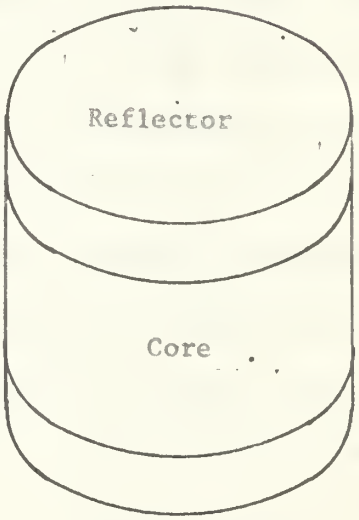

Figure 6(c)

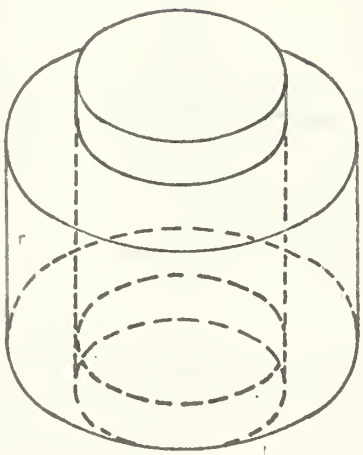

Figure 6(d)

Figure 6 Geometries for Analytical Solutions

is not included in the calculations thus far for comparison purposes) was "neutron spectrum hardening". This additional factor, resolves the problem of not predicting the correct critical mass.

Spectrum hardening refers to a shift of the curve for neutron distribution as a function of energy towards higher energies. When the moderating material has a constant scattering cross section over the thermal energy range, the shift is due to the $\frac{1}{v}$ or approximately $\frac{1}{v}$ absorption cross section of nuclides contained. In such cases, the shift is slight if the absorber concentration is not large. When the scattering cross section changes significantly in the thermal range due to effects of molecular binding, the spectrum is further hardened. Recent papers [1,2,3] indicate that for polyethylene moderated assemblies, the shift is very significant and leads to lower averaged macroscopic cross sections. Neglecting this effect can result in a large difference in the criticality determinant. The spectrum shift in water can be predicted quite accurately using Nelkin's Kernel[4], but no kernel has been developed for polyethylene.

[1] D. R. Bach, S. I. Bunch, J. R. Roesser and R. E. Slovacek, Low Energy Neutron Spectra Measurements in Polyethylene Moderated Media, Transactions of American Nuclear Society, Vol. 3, No. 2, Dec. 1960.

[2] J. R. Beyster, J. L. Wood and H C. Honek, Spatially Dependent Neutron Spectra, Transactions of American Nuclear Society, Vol. 3, No. 2, Dec. 1960.

[3] J. R. Beyster, J. L. Wood, W. M. Lopez and R. B. Walton, Measurements of Neutron Spectra in Water, Polyethylene and Zirconium Hydride. Nuclear Science and Engineering, Vol. 9, No. 2, Feb. 1961.

[4] M. Nelkin, "Scattering of Slow Neutrons by Water", Physics Review, 119, 1960.

A survey of the papers on this subject for polyethylene-moderated assemblies indicated that the peak of the distribution should occur at 0.029 or 0.030 electron volts for the absorber to scatterer ratio of the AGN 201 core material (the unshifted spectrum peak is at 0.0253 electron volts for 20°C). In calculating macroscopic cross sections averaged over this shifted spectrum, an effective neutron temperature of 336°K to 347°K would be used. These effective neutron temperatures correspond to ratios of average neutron velocity to the 2,200 meter/sec value of 1.21 to 1.23 as compared to 1.128 for an unshifted spectrum. The empirical formula (1)

$$\frac{\bar{v}}{v} = 1.128 + 1.36\,\frac{\Sigma_a(k_oT)}{\xi\Sigma_s}$$

where $\bar{v}$ is the average neutron velocity of the distribution and v is the velocity corresponding to energy k_oT yields a value of 1.23 which tends to confirm the data taken from spectrum plots. For purposes of calculation, assume for $\frac{1}{v}$ absorbers

$$\bar{\sigma} = \frac{1}{1.128}\sqrt{\frac{T_o}{T_{eff}}}\,\sigma_{2200} \qquad T_o = 293°K$$

$$= \frac{1}{1.22}\sqrt{\frac{T_o}{T}}\,\sigma_{2200}$$ where T is the actual temperature

Applying this equation to recalculation of the macroscopic cross sections of the core materials,

$$\bar{\Sigma}_a^{235} = .0781 \text{ cm}^{-1}$$

$$\bar{\Sigma}_f^{235} = .0646 \text{ cm}^{-1}$$

$$\bar{\Sigma}_a = .0214 \text{ cm}^{-1}$$ for carbon, oxygen and hydrogen combined

$$\eta f = 1.590$$

$$k_\infty = 1.527$$

Comparing to the previous calculated values, the effect on k_∞ is slight, but the absorption and fission macroscopic cross sections are decreased roughly seven or eight percent. The thermal diffusion coefficient would also be affected by a spectrum shift, but the value for water from which it was estimated is an experimental value and must then include this effect. The value of 0.125 cm for the thermal diffusion coefficient of polyethylene is at best a guess in any event.

(e) Two-Group Parameters Which Predict Correct Critical Mass

The two-group parameters[1] after all corrections are summarized in Table 4.

Table 4

Two Group Nuclear Parameters

$D_1 = 0.623$ cm	$\tau_c = 19.7$ cm^2	$k_\infty = 1.527$
$D_2 = 0.125$ cm	$\Sigma_a^{(2)} = 0.0995$ cm^{-1}	$p_c = 0.960$
$D_3 = 0.929$ cm	$\tau_r = 304$ cm^2	$p_r = 1.00$
$D_4 = 0.838$ cm	$\Sigma_a^{(4)} = 0.000374$ cm^{-1}	

Assuming an effective reflector thickness of 30 cm[2], these parameters predict for spherical geometry a core radius of 14.2 cm., a critical volume of approximately 12,000 cm^3 which is just less than the actual critical volume and an extrapolated radius of approximately 8 inches, slightly

[1] For computational purposes, three figure precision is assumed, but the data does not justify this degree of precision.

[2] The graphite is 20 cm thick, but the lead and water make some contribution to neutron reflection.

greater than that indicated in the flux plot (which would be expected for an equivalent sphere approximation). The parameters then may not be quite correct, but are reasonably close to correct values.

(f) Temperature Coefficient of Reactivity, Delayed Neutron Effectiveness and Neutron Lifetime.

Using the parameters derived for the two-group analysis, several other parameters can be estimated. As a check on the experimental value of the temperature coefficient of reactivity, an analytical value may be calculated using the method of Reference (2). From the equation

$$k_{eff} = \eta f \varepsilon p P_f P_s$$

we obtain

$$\frac{1}{k}\frac{\partial k}{\partial T} = \frac{1}{\eta}\frac{\partial \eta}{\partial T} + \frac{1}{f}\frac{\partial f}{\partial T} + \frac{1}{\varepsilon}\frac{\partial \varepsilon}{\partial T} + \frac{1}{p}\frac{\partial p}{\partial T} + \frac{1}{P_f}\frac{\partial P_f}{\partial T} + \frac{1}{P_s}\frac{\partial P_s}{\partial T}$$

With the data available and using plots of various parameters as a function of temperature as required:

$$\frac{1}{\varepsilon}\frac{\partial \varepsilon}{\partial T} \approx 0$$

$$\frac{1}{f}\frac{\partial f}{\partial T} = (1-f)\left[\frac{1}{\overline{\Sigma}_{aF}}\frac{\partial \overline{\Sigma}_{aF}}{\partial T} + \frac{1}{2T}\right] = -4.2 \times 10^{-5}/^{\circ}C$$

$$\frac{1}{\eta}\frac{\partial \eta}{\partial T} = -\frac{1}{1+a'}\frac{\partial (1+a')}{\partial T} - \frac{1}{f_{1+a}}\frac{\partial f_{1+a}}{\partial T} = 4.0 \times 10^{-5}/^{\circ}C$$

$$\frac{1}{P_f}\frac{\partial P_f}{\partial T} = -(1-P_f)\left[\frac{2}{\ell_r}\frac{\partial \ell_r}{\partial T} + \frac{1}{1-f}\frac{\partial f}{\partial T} - 6a_0 - \frac{1}{2T}\right] = -7.9 \times 10^{-5}/^{\circ}C$$

$$\frac{1}{P_s}\frac{\partial P_s}{\partial T} = -(1-P_s)\left[\frac{1}{T}\frac{\partial T}{\partial T} + \frac{1}{B^2}\frac{\partial B^2}{\partial T}\right] = -31.9 \times 10^{-5}/^{\circ}C$$

$$\frac{1}{p}\frac{\partial p}{\partial T} = \frac{\overline{\Sigma}_{aF}}{T\left[\sum N_F \sigma_{PF} + (N\sigma_s)_0\right]} = 14.1 \times 10^{-5}/^{\circ}C$$

$$\frac{1}{k}\frac{\partial k}{\partial T} = -25.9 \times 10^{-5}/^{\circ}C$$

$$C_T \approx \frac{1}{k} \frac{\partial k}{\partial T}$$

$$C_T \approx -2.6 \times 10^{-4}/^{\circ}C$$

$$C_{T_{exp}} \approx -2.75 \times 10^{-4}/^{\circ}C$$

The value of C_T compares quite well with the experimental value, but depends heavily on the Fermi Age of the core material which is not well known. Also, the theory is based on an equivalent bare reactor and neglects any effects contributed by the reflector.

The overall effectiveness of delayed neutrons β can be estimated from the fast leakage and resonance escape probability. Delayed neutrons are emitted with an average energy of 0.515 Mev (1) whereas prompt neutrons have an average energy of 2 Mev. The resonance range for Uranium-238, which is the chief resonance absorber, lies below 0.515 Mev. The resonance escape probabilities should then be the same for delayed and prompt neutrons. Fast leakages for both types of neutrons would also be similar for materials to which the Fermi Age theory may be applied, since the age is assumed to vary almost linearly with lethargy. For hydrogenous moderators the continuous slowing down model does not apply, and the age to Indium resonance in water for an initial neutron energy of 0.97 Mev. is roughly half the age for the prompt neutrons.[1] Since 0.97 Mev. is representative of the delayed neutron initial energies, the ratio of fast leakage of the delayed neutrons to that of the prompt neutrons is by the two-group approach approximately

[1] D. Graham Foster, Jr., Age of Na-Be Neutrons in Water and Kerosene, Nuclear Science and Engineering, Vol. 8, No. 2, Aug. 1960.

$$\frac{\frac{1}{1+\tau_d B^2}}{\frac{1}{1+\tau_f B^2}} \approx \frac{\frac{1}{1+10.6\times 0.024}}{\frac{1}{1+19.7\times 0.024}} = 1.17$$

The delayed neutron effectiveness then is probably slightly greater than 1.17 since the above estimate of the age for delayed neutrons is too large.

One other nuclear parameter that will be required is the neutron lifetime. For thermal neutrons, this is given approximately by the formula

$$\Lambda = \frac{1}{\Sigma_a \bar{v}\left(1 + L^2 B^2\right)}$$

Slight corrections are necessary to include the fast neutron lifetime in the overall neutron lifetime. The method of correction and the correction used are given in Section 7.

6. Heat Transfer Calculations.

The relative rates of heat generation in the core and heat transfer from the core at any time set limits on the future capability of the reactor. The heat generation rate is a function of the neutron flux; the heat transfer rate is a function of temperature. With a high neutron flux and a corresponding high heat generation rate, the temperature rises towards a value where the heat transfer rate balances the heat generation rate. The temperature rise however has an adverse effect on nuclear parameters such that the ability to maintain or to increase power is reduced as the temperature increases.

In specifying the heat generation rate in the core, it is assumed that each fission of a fuel atom creates a certain amount of energy realized in the form of heat. The value frequently used is 200 Mev. per fission although various values between 190 Mev. and 200 Mev. are reported. About 90% of the energy is produced at the time of fission; the remainder, resulting from the decay of fission products, is produced at a rate dependent on fission product decay constants. The heat generated then is not instantaneous, nor is it localized. Depending on the size and construction of a reactor, a certain percentage of the heat is produced in each of the fuel, moderator and shield regions. For a small thermal reactor, about 90% of the heat is produced in the fuel and moderator, the remainder in the reflector and shielding. (1) For computer solutions, it will be assumed that about 90% of the energy of the fissions appears in a very short time in the form of heat in the core.

In an analysis of the heat transfer from the core, effects such as eddy currents in the air gaps and the reduction of thickness of air gaps

due to thermal expansion are negligible. Over the temperature range of interest, the heat transfer is by conduction and the variation of thermal conductivity with temperature can be disregarded. These assumptions lead to a heat transfer rate which is a linear function of the temperature difference between the core and whichever region remote from the core is assumed to remain at a steady temperature.

The water tank containing half a ton of water could absorb all the heat generated by the reactor operating at 1,000 watts for one hour with less than a two degree centigrade temperature rise. With only short periods at high power envisaged, the water tank serves as the heat sink for analysis purposes. Working inward towards the core, the temperature difference through the lead may be estimated assuming a spherical shell for which

$$T_i - T_o = \frac{q}{4K}\left(\frac{1}{r_i} - \frac{1}{r_o}\right)$$

Using a conductivity for lead of 20 BTU/hr-ft-°F, the temperature difference is about three degrees Fahrenheit per kilowatt of power. Similarly, for the graphite, a temperature difference is estimated as 3.7°F per kilowatt of power assuming a conductivity of 109 BTU/sec-ft°F[1].

Next, since the temperature coefficient of reactivity mentioned in Section 4 is based on the average temperature of the core, the relation between average core temperature above the core surface temperature and the heat flow from the core is required. A first approximation may be

[1]The conductivity for graphite (with a density of 1.75 gm/cc) parallel to direction of extrusion is about 0.55 cal/sec-cm-°C (1). Perpendicular to the direction of extrusion, the conductivity is less by 30 to 50%. The value 0.45 cal/sec-cm-°C is taken as a mean.

obtained assuming a spherical core with a thermal flux distribution varying as

$$\phi_{th} = C \frac{\sin \frac{\pi r}{R_e}}{\frac{\pi r}{R_e}} \quad \text{where } C \text{ is a constant}$$

From the equation

$$\nabla^2 T(r) = \frac{1}{r^2}\frac{\partial}{\partial r}\left(r^2 \frac{\partial T}{\partial r}\right) = -\frac{\dot{q}(r)}{K} = -\frac{\dot{q}_o}{K} \frac{\sin \frac{\pi r}{R_e}}{\frac{\pi r}{R_e}}$$

$$T(r) = T_o - \frac{\dot{q}_o}{k\left(\frac{\pi}{R_e}\right)^2}\left[1 - \frac{\sin \frac{\pi r}{R_e}}{\frac{\pi r}{R_e}}\right]$$

Then the total heat produced in the core per unit time is

$$\dot{Q} = \int_0^{r_1} \dot{q}_o \frac{\sin \frac{\pi r}{R_e}}{\frac{\pi r}{R_e}} dV$$

$$= \frac{4\pi \dot{q}_o}{\left(\frac{\pi}{R_e}\right)^3}\left(\sin \frac{\pi r_1}{R_e} - \frac{\pi r_1}{R_e} \cos \frac{\pi r_1}{R_e}\right)$$

and the average temperature over the core is

$$\bar{T} = T_o - \frac{\dot{q}_o}{k\left(\frac{\pi}{R_e}\right)^2}\left[1 - \int_0^{r_1} \frac{\sin \frac{\pi r}{R_e}}{\frac{\pi r}{R_e}} dV\right]$$

$$= T_o - \frac{\dot{q}_o}{k\left(\frac{\pi}{R_e}\right)^2}\left[1 - \frac{3}{\left(\frac{\pi r_1}{R_e}\right)^3}\left(\sin \frac{\pi r_1}{R_e} - \frac{\pi r_1}{R_e} \cos \frac{\pi r_1}{R_e}\right)\right]$$

Relating the difference between average and surface temperature to the heat generation with R_e = 20 cm, r_1 = 14.2 cm and using a conductivity for polyethylene of 8×10^{-4} cal/sec-cm-°C,

$$\frac{\bar{T} - T_{r_1}}{\dot{Q}} = 0.209\ ^\circ F/Btu/hr$$

Neglecting contact resistances and air gaps at this point, the average temperature of the core would be over 700°F greater than the surface temperature if steady state operation at 1 kilowatt were possible. The temperature drop across the lead and graphite is therefore negligible and based on this model, a net thermal conductance of approximately 4.7 BTU/hr-°F may be assigned.

The spherical core model does not take into account the various heat paths in the actual construction such as the glory hole casing and the aluminum control rod casings. Some indication of their significance can be obtained by considering a network consisting of the flow paths between the various core components and the thermal resistance of the paths. Considering each disc of the core separately and assuming a radial flux distribution proportional to the Bessel function J_o, the resistance to radial heat flow may be obtained from

$$K\nabla^2 T(r) + \dot{q}_o J_o(\alpha r) = 0 \quad \text{where} \quad \alpha = \frac{2.4048}{R_e}$$

or

$$\frac{1}{r}\frac{\partial}{\partial r}\left(r\frac{\partial T}{\partial r}\right) = -\frac{\dot{q}_o}{K}\left[1 - \frac{(\alpha r)^2}{2^2(1!)^2} + \frac{(\alpha r)^4}{2^4(2!)^2} - \frac{(\alpha r)^6}{2^6(3!)^2} + \cdots\right]$$

Letting $Z = \frac{\alpha r}{2}$ and $dZ = \frac{\alpha}{2}dr$

$$T_o - T_r = \frac{\dot{q}_o}{K\left(\frac{\alpha}{2}\right)^2}\left[\frac{Z^2}{2^2} - \frac{Z^4}{4^2(1!)^2} + \frac{Z^6}{6^2(2!)^2} - \cdots\right]$$

$$\dot{Q} = \int_o^{r_1} \dot{q}_o J_o(\alpha r)\, dV$$

$$= \frac{2\pi h \dot{q}_o}{\left(\frac{\alpha}{2}\right)^2}\left[\frac{Z_1^2}{2} - \frac{Z_1^4}{4(1!)^2} + \frac{Z_1^6}{6(2!)^2} - \cdots\right]$$

$$T_o - \bar{T} = \int_o^{r_1} \frac{\dot{q}_o}{K\left(\frac{\alpha}{2}\right)^2}\left[\frac{Z^2}{4} - \frac{Z^4}{16(1!)^2} + \frac{Z^6}{36(2!)^2} \cdots\right]$$

$$= \frac{\dot{q}_o r_1^2}{4K}\left[\frac{1}{2!} - \frac{Z^2}{2!3!} + \frac{Z^4}{3!4!} - \frac{Z^6}{4!5!} + \cdots\right]$$

Substituting the core radius r_1 = 12.9 cm, the extrapolated radius R_e = 18.8 cm (from two-group analysis) and the conductivity of polyethylene

$$\frac{\bar{T} - T_{r_1}}{\dot{Q}} = \frac{0.2+8}{11} \ ^\circ F/Btu/hr$$

From blueprints of the core region of Figure 2, there is an air gap between the sides of the core and the graphite approximately equal to 0.1 inches. At the top, there is a gap of approximately one-quarter inch. The bottom disc rests on a graphite block. The aluminum thimbles and casings of the control rods provide a net area for heat flow downwards of about 1.3 square inches but have air gaps around them of approximately 0.1 inches which tend to hinder heat flow to the rods. Further heat paths are the glory hole casing and the divider plate between the top and bottom half of the core.

Combining the components and resistances between them, including air gaps and contact resistance, the network of Figure 7 is obtained. Contact resistances were included on the basis of h_c = 500 BTU/hr-ft^2-°F. Each core disc can lose heat to the next disc, radially to the graphite, or to an aluminum component if it is near one, and receives heat according to its size and to an assumed cosine axial distribution of the heat generation rate.

The network can be solved by the relaxation technique or a matrix inversion. The latter method was chosen, and for an arbitrarily chosen overall heat generation rate, the temperatures at each point and the heat flows along certain paths were determined. Results of the analysis indicated that about 70% of the heat flows directly to the graphite out the top, sides and bottom of the core, the remainder through the various paths offered by the aluminum components. Temperatures in the top half of the core are higher than in the bottom half due to the lack of aluminum paths and the poor conductivity of the air gap at the top as compared to pure contact resistance at the bottom. The overall average temperature for

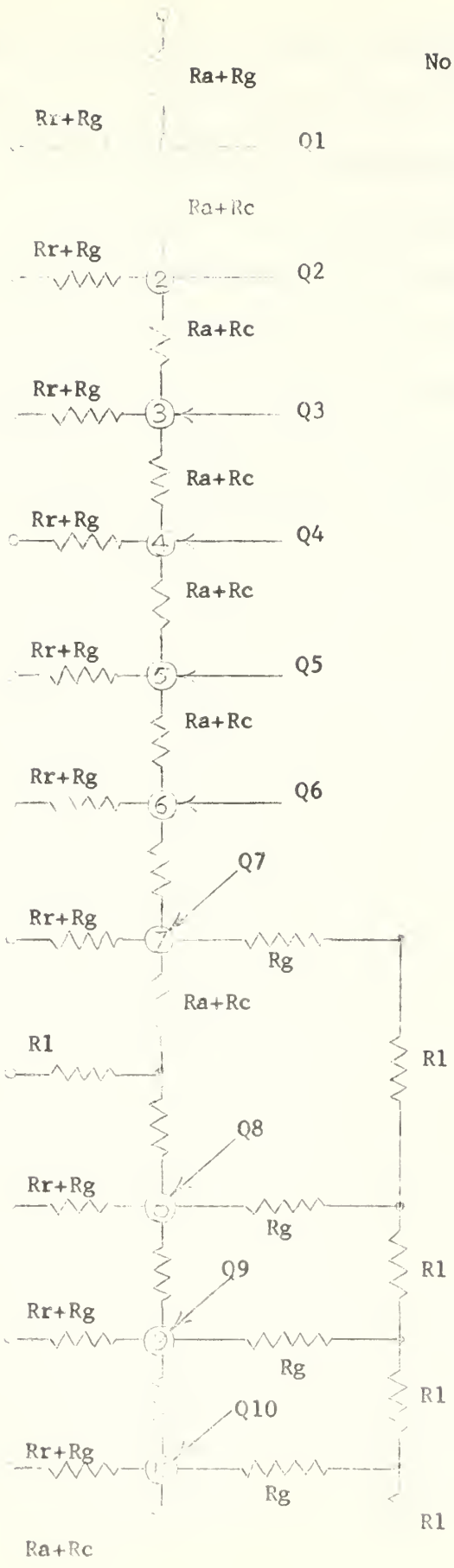

Notation:

(1)	Core disc
	Point at temperature of surroundings
	Point in structural material heat flow path
Ra	Axial thermal resistance
Rc	Contact resistance
Rg	Air gap resistance
Rl	Thermal resistance of aluminum
Rr	Radial Thermal resistance
Q	Heat Generation rate in core disc

Figure 7 Heat Transfer Network for Core Components

an assumed 1,000 BUT/hr total heat generation rate was over 100°F corresponding to a conductance for the core slightly less than 10 BTU/hr-°F. This value of conductance is about twice that obtained for the spherical approximation. It is quite probable that this approximation over-estimates the significance of the aluminum components and that the actual conductance is bracketed by the two approximations.

Since it is anticipated that the temperature coefficient for a rapid rise of power would be greater than the experimentally determined value, the lower estimate of conductance is favored for partial compensation.

7. Computer Solution of the Coupled Differential Equations.

The equation for the neutron density at a point in the reactor if prompt and delayed neutrons are treated equivalently is:[1]

$$\frac{dn}{dt} = \left(\frac{k_{eff}-1}{\Lambda}\right)n - \frac{k_{eff}\beta n}{\Lambda} + \sum \lambda_i C_i$$

(Appendix 1, Eqn. 1)

If the delayed neutron effectiveness is included and the assumptions of Appendix 1 are used, this becomes:

$$\frac{dn}{dt} = \frac{k_{eff}\gamma}{\Lambda}\left(\frac{\rho}{\gamma} - \beta\right)n + \sum \lambda_i C_i$$

where ρ is the effective reactivity at any temperature. With the temperature dependence of the reactivity displayed, this becomes:

$$\frac{dn}{dt} = \frac{k_{eff}\gamma}{\Lambda}\left(\frac{\rho}{\gamma} + \frac{C_T\Delta T}{\gamma} - \beta\right)n + \sum \lambda_i C_i$$

where ρ is the effective reactivity at an arbitrary reference temperature and ΔT is the difference between the temperature of the core and the reference temperature. The corresponding equations for the six delayed neutron group precursors have the form:

$$\frac{dC_i}{dt} = -\lambda_i C_i + \frac{k_{eff}\gamma\beta_i}{\Lambda} n$$

The temperature dependence equation, assuming an average temperature in the core is:

$$\frac{d(\Delta T)}{dt} = \frac{\bar{\Sigma}_f \bar{\nu} e \mathcal{V}}{\rho_o C} n - \frac{K_o(\Delta T)}{\rho_o C}$$

where e is the energy released per fission expressed in units of heat and K_o is the conductance of the core based on average core temperature

[1]The Ra - Be neutron source in the reactor is neglected since the contribution to overall neutron density is small.

(See Section 6).

The eight coupled differential equations then have the form

$$\frac{dn}{dt} = G\left(\frac{\rho}{\delta} + \frac{c_T \Delta T}{\delta} - \beta\right) n + \sum \lambda_i C_i$$

$$\frac{dC_i}{dt} = -\lambda_i C_i + G\beta_i n$$

$$\frac{d(\Delta T)}{dt} = Fn - \frac{K_o}{\rho_o c}(\Delta T)$$

where

$$F = \frac{\bar{\Sigma}_f \bar{v} e \bar{V}}{\rho_o c} \qquad G = \frac{k_{eff} \gamma}{\Lambda}$$

These equations cannot be solved analytically, and analog computer solutions are limited to relatively small variations of any of the dependent variables unless special provisions are made. Using numerical methods, digital computer solutions for large variations can be obtained with any of a number of integration techniques.

Of these techniques, the Euler method, modifications of Euler's method and the Runga-Kutta method are frequently used. The Euler method consists of computing each new point on the basis of the last point and the slope of the function evaluated at that point:

$$y_1 = y_o + \left(\frac{dy}{dx}\right)_{x_o, y_o} \Delta x_{o \to 1}$$

An improvement of Euler's method consists of computing an estimated value and providing an improvement by averaging the slopes for last point and the estimated next point;

$$y_1^* = y_o + \left(\frac{dy}{dx}\right)_{x_o, y_o} \Delta x_{o \to 1}$$

$$y_1 = y_o + \frac{1}{2}\left[\left(\frac{dy}{dx}\right)_{x_o, y_o} + \left(\frac{dy}{dx}\right)_{x_1, y_1^*}\right] \Delta x_{o \to 1}$$

Both the Euler and modified Euler techniques lack the smoothness of the Runga-Kutta technique which consists of computing several estimated values

and averaging the values according to a numerical technique (3). Other methods provide greater improvement, but with more complexity. The Milne method and the Hamming method base calculations for a point on the value and slope of three previous points as well as applying a "corrector" and "modifier" formula.

The coefficients of the equations to be solved are calculated from data in the preceeding three sections. These data are summarized in Table 5. The delayed neutron parameters are listed in Table 6. Using a specific heat of polyethylene of 0.55 cal/gm-°C and a specific heat of uranium dioxide of 0.057 cal/gm-°C, the following values are obtained for the coefficients corresponding to the case of maximum reactivity input:

$$F = \frac{\bar{\Sigma}_f \bar{\nu} e \mathcal{N}}{\Sigma(\rho_o C)} \times 90\% = 2.31 \times 10^{-7} \text{°C/sec-neutron/cm}^3$$

$$\frac{K_o}{\rho_o C} = K_o / \Sigma(\rho_o C) = 1.0 \times 10^{-4} \text{ sec}^{-1}$$

$$\frac{\rho}{\delta} = 6.79 \times 5.6 \times 10^{-4} = 3.81 \times 10^{-3}$$

$$\frac{d}{dt}\left(\frac{\rho}{\delta}\right) = 0.439 \times 5.6 \times 10^{-4} = 2.46 \times 10^{-4}/\text{sec}$$

$$\Lambda = \frac{1}{\bar{\Sigma}_a \bar{v}(1+L^2B^2)} + \frac{1}{\Sigma_r \bar{v}_f (1+\tau B^2)} = 41 \times 10^{-6} \text{ sec}$$

$$G = \frac{k_{eff}\,\gamma}{\Lambda} = 2.8 \times 10^{4} \text{sec}^{-1}$$

Before attempting a solution with the maximum reactivity input values, a program was written based on Euler's method for the National Cash Register Company Model 102-A digital computer to establish a comparison between a computer solution and the experimental results for the small negative step in reactivity mentioned in Section 4. A conclusion was soon reached that these equations could not be solved satisfactorily with a relatively slow computer. The small time increments which were used required excessive computer time for the calculation of points and larger

Table 5

Summary of Experimental and Calculated Data

Temperature Coefficient of Reactivity		$= 2.75 \times 10^{-4}$/°C
Position of coarse rod at reference temperature of 20°C with polyethylene in glory hole		= 17.91 cm (Fig. 3)
Worth of coarse rod in units of reactivity		$= 5.6 \times 10^{-4}$/cm.
Rate of coarse rod insertion		= 26.3 ± .02 cm/min
Position of coarse rod when fully inserted		= 24.70 cm.
Delayed neutron effectiveness factor		= 1.17
Macroscopic absorption cross section		$= 0.0781$ cm^{-1}
Macroscopic fission cross section		$= 0.0646$ cm^{-1}
Average slow neutron velocity		= 2680 m/sec
Geometric buckling	B^2	$= 0.024$ cm^{-2}
Slow diffusion coefficient	D_2	= 0.125 cm
Fast diffusion coefficient	D_1	= 0.623 cm
Fermi Age, (or fast diffusion length)	τ	$= 19.7$ cm^2
Conductivity of core	4.7 Btu/hr/°F < K < 10 Btu/hr/°F	
Density of polyethylene		= 0.909 gm/cc
Density of Uranium dioxide		= 0.313 gm/cc

Table 6

Delayed Neutron Parameters

$\beta_1 = 0.00021$	$\lambda_1 = 0.0124\ sec^{-1}$
$\beta_2 = 0.00140$	$\lambda_2 = 0.0305\ sec^{-1}$
$\beta_3 = 0.00125$	$\lambda_3 = 0.111\ sec^{-1}$
$\beta_4 = 0.00253$	$\lambda_4 = 0.301\ sec^{-1}$
$\beta_5 = 0.00074$	$\lambda_5 = 1.14\ sec^{-1}$
$\beta_6 = 0.00027$	$\lambda_6 = 3.01\ sec^{-1}$

time increments led to instability.

Since the basic service library of the Control Data Corporation 1604 digital computer contains a Runga-Kutta-Gill[1] subroutine for the simultaneous solution of coupled differential equations, the program for a negative step in reactivity was re-written in Neliac Compiler language[2] to take advantage of the faster computer and a smoother integration method.

A number of runs to determine neutron density as a function of time for a step reactivity of -2.21×10^{-3} were made with this program to determine suitable time increments[3] for the method and the effect of changing neutron lifetime for which the calculated value of 41 microseconds seemed too small. The results of these runs are shown in Fig. 8

[1]The Runga-Kutta-Gill method is an adaption of the Runga-Kutta method for computer use.

[2]The Neliac Compiler originated with the Navy Electronics Laboratory in San Diego and was adapted for use on the CDC 1604 computer in 1960.

[3]Although increments for the independent variable can be calculated in some cases to provide solutions within specified error limits, it is more practiced to duplicate a run with 1/2 the selected increment and compared solutions for satisfactory error.

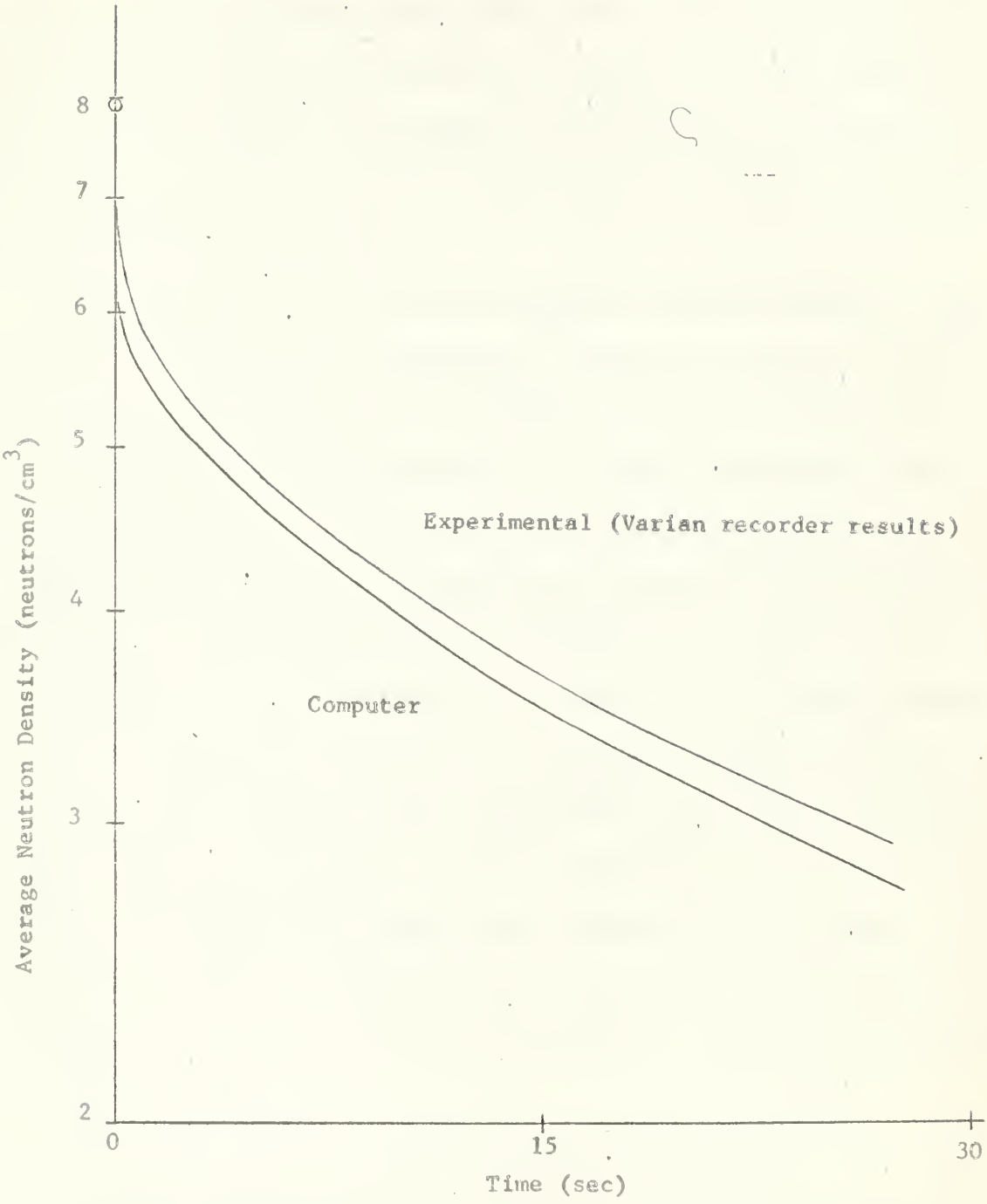

Figure 8 Comparison of Computer Solution with Experimental Results for a Negative step in Reactivity

with a single curve, since it was found that time increments from 0.001 sec to 0.01 sec provided the same data to four figure accuracy and the magnitude of neutron lifetime could be doubled with little effect. The computer solution is almost exactly five per cent low which, in view of the approximations and experimental data involved, is within acceptable limits. The discrepancy is attributed to the difference between an experimentally approximate step input and the numerical method technique application for an actual step.

Using the same method as for the negative transient program, a new program was written to solve the kinetic equations for ramp and step inputs, with or without temperature dependence. Details of this program are given in Appendix 2. The coefficients obtained previously in this section when supplied to this program lead to the curves shown in Fig. 9. (Again it was found that the magnitude of neutron lifetime had negligible effect). The neutron density corresponding to 1,000 watts is indicated by a horizontal line and it can be seen that the program indicates a capability considerably in excess of this power. However, this solution assumes that absorbers, which would reduce the available reactivity, are absent from the glory hole. The power during this transient period remains above 1,000 watts for approximately two and a half minutes. If the reactor were held at a thousand watts such that the heat generation were constant, the temperature would increase at a slower rate and provide longer operating time.

The program was re-run with a reactivity corresponding to that available with the glory hole empty. The results are shown in Fig. 10. It can be seen that a longer time is required to reach high powers and that

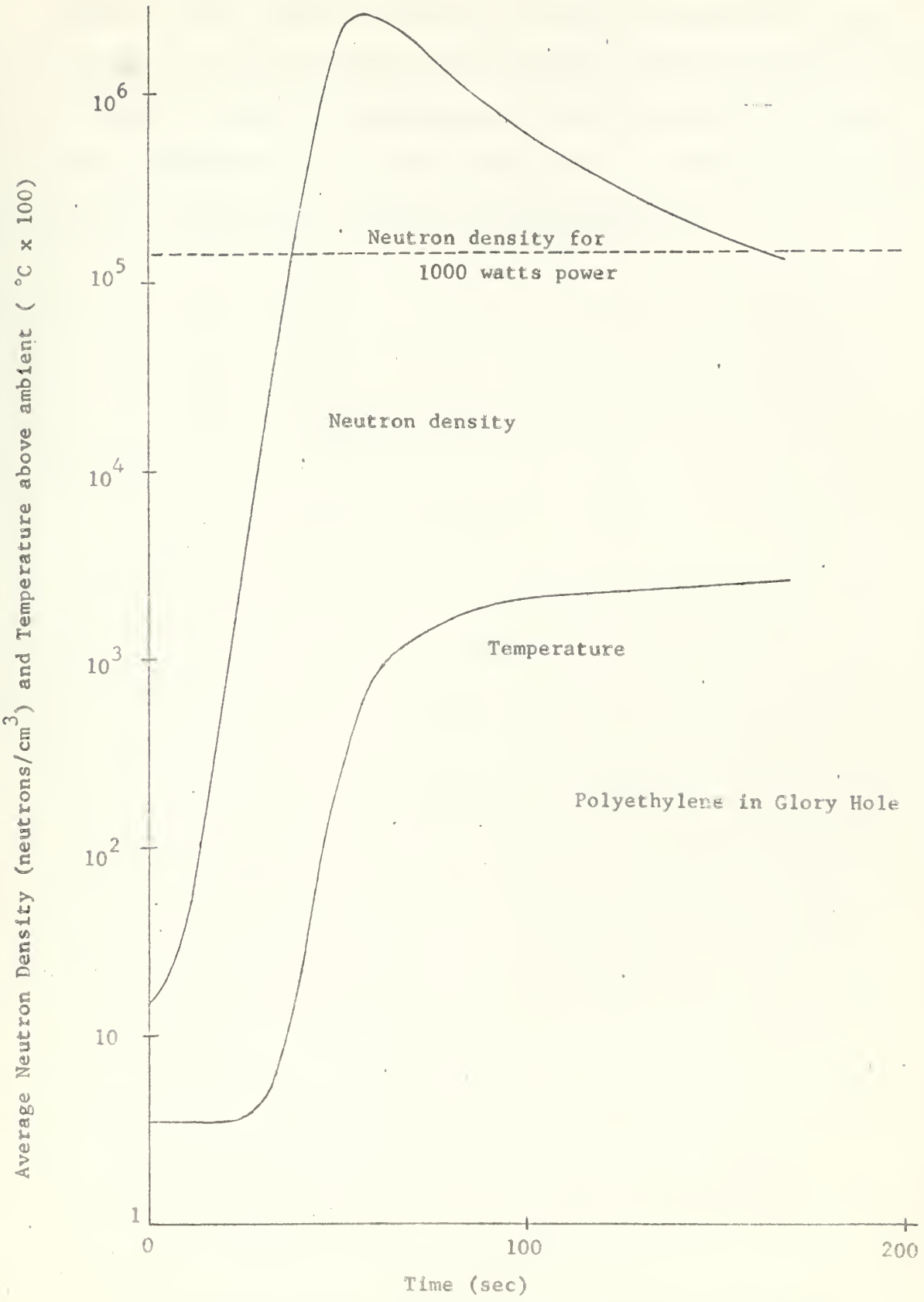

Figure 9 Neutron Density and Temperature for Maximum Reactivity Ramp Input

the temperature is higher when 1,000 watts is achieved. Operating time is reduced, but the difference in reactivity between this case and the case where the glory hole was filled with polyethylene represents a reasonable amount of absorber which can be irradiated. The reactor period during the rise in power agrees within a fraction of a second with the experimental value for the same reactivity.

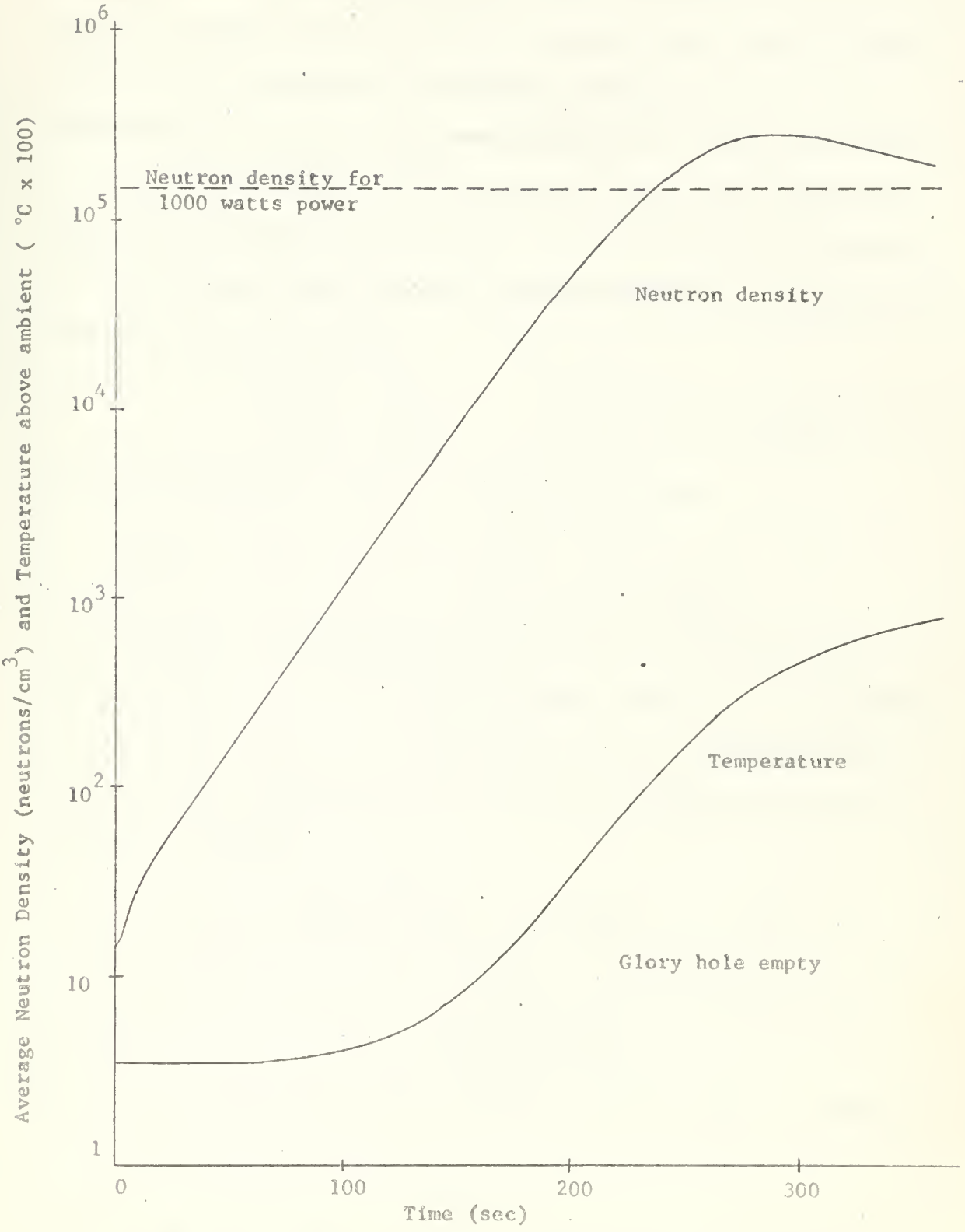

Figure 10 Neutron Density and Temperature for Maximum Reactivity ramp Input.

8. A Two-Group-Computer Solution.

A computer solution to solve the simultaneous partial differential equations for the reactor was written with the intention of obtaining the flux at every point for checking parameters and to provide initial conditions for a space and time dependent transient solution. The transient problem, however, was never written as it became evident that excessive computer time would be required to achieve any results with the approach envisaged. The reason for this may be seen from considering the following finite difference equation example.(3) From the time dependent diffusion equation

$$A^2 \frac{\partial^2 V}{\partial x^2} = \frac{\partial V}{\partial t} \qquad \text{where } V \text{ is a variable}$$

the finite difference equation is obtained as follows

$$v_{m,n+1} = S v_{m+1,n} - (1-2S) v_{m,n} + S v_{m-1,n}$$

If "S" exceeds 1/2, the presence of round off or truncation errors causes exponentially increasing oscillations. The value of "S" depends on the mesh size chosen and in the case of cylindrical geometry with a radial and axial mesh spacing " Δ " of one centimeter and a time increment " Δt" where

$$\phi_{1\,i,j}^{t+1} = \phi_{1\,i,j}^{t} + \frac{\Delta t \nu D}{\Delta^2}\left[a\phi_{1\,i+1,j}^{t} + b\phi_{1\,i-1,j}^{t} + c\phi_{1\,i,j+1}^{t}\right.$$
$$\left. d\phi_{1\,i,j-1} + 4\phi_{1\,i,j}^{t}\right] - \Delta t \Sigma_r^{(1)} \phi_{1\,i,j}^{t} + \Delta t \nu \Sigma_f \phi_{2\,i,j}$$

we obtain $$1 - \Delta_t \Sigma_r^{(1)} - \frac{4\Delta t \nu D}{\Delta^2} > 0$$

the velocity in the fourth term results in a time interval t which is very small. Roughly

$$\frac{4 \times \Delta t \times 220000 \times 0.125}{1 \times 1} < 1$$

$$\Delta t < 9 \times 10^{-6} \text{ sec}$$

The computer would have to work through the mesh system for each neutron group 110,000 times to reach the first second of simulated time which would require many minutes of computer time. Other approaches might be practical, but to December 1960, only spherical geometry programs have been published.

The time-independent partial differential equation program was written to use the Peaseman Rackford method[1] as used in CURE[2]. An outline of the program is given in Appendix 3. Results were not satisfactory in that convergence was poor and instabilities occured which rapidly increased in magnitude. For initial values, a cosine distribution in the core and a linear distribution in the reflector were used and the first few passes tended to smooth this data towards the experimental points as shown in Figure 11. However, during subsequent passes, a hump developed at the core reflector interface and was rapidly amplified. The hump is shown in Fig. 11, after the program had been operated ten times.

[1] D. W. Peaceman and H. H. Rackford, Jr., "The Numerical Solution of Parabolic and Elliptic Differential Equations J. Soc. Industrial and Applied Math 3, 1955.

[2] E. L. Wachspress CURE A Generalized Two Space Dimension Multigroup Coding of the 704 KAPL - 1724, May 1957.

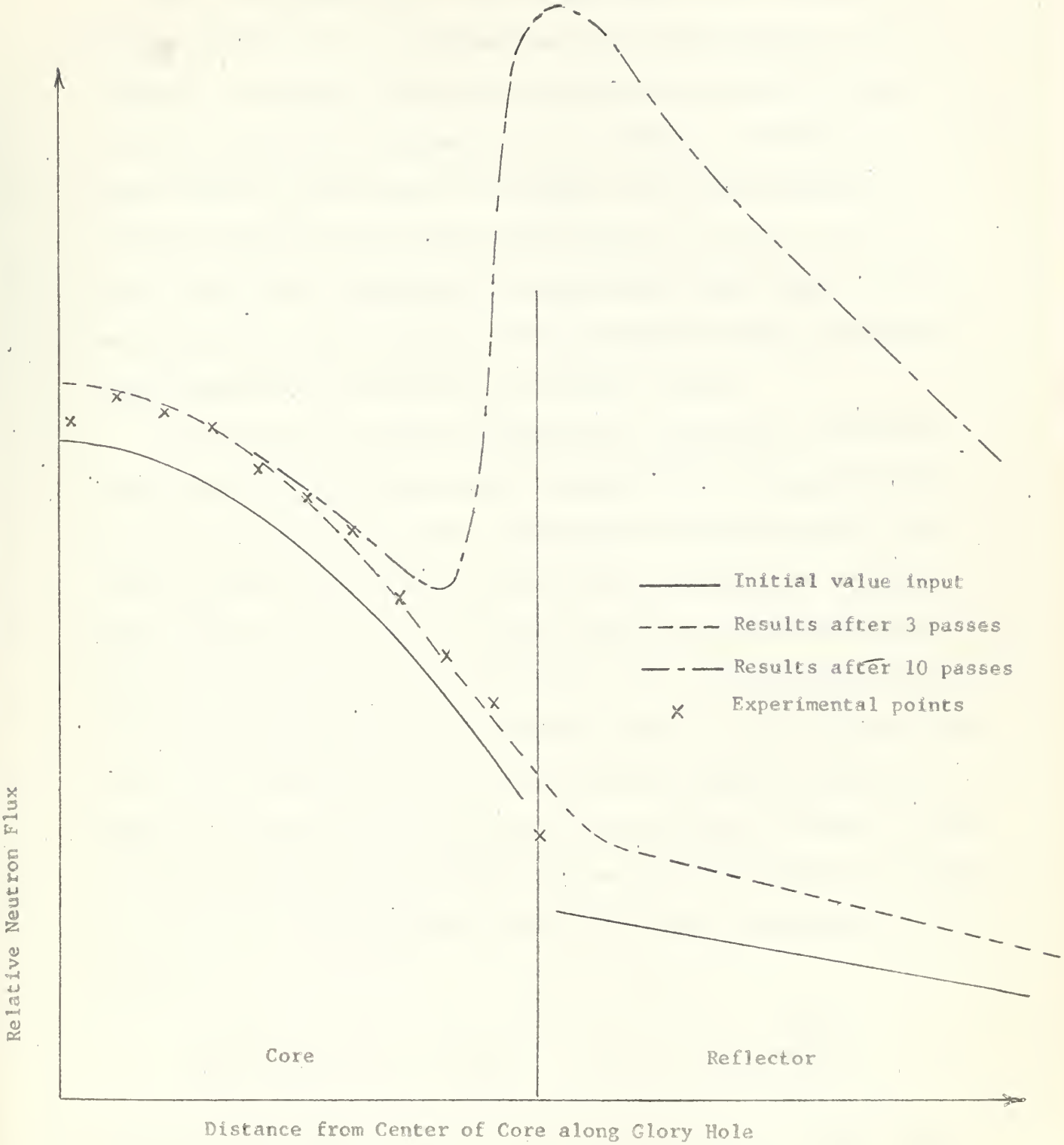

Figure 11 - Two-Group Two-Region Computer Solution for Time Independent Neutron Flux

9. Discussion and Conclusions

Much of the data used in this investigation lack precision, and the methods used are approximations with varying degrees of reliability. In general, trends can be predicted but absolute values of neutron density and temperature are not reliable. Temperature values should be within about ten percent if the neutron density is correctly predicted, but neutron density might be off by a factor of two at high powers. Comparison with experimental data, where possible, was found to be quite reasonable, but experimental tests of the high power behaviour are prevented by the present license.

In view of the reasonable agreement with experimental data where checks were made, predictions using the same basic data should not be too amiss. On this presumption, the computer solutions indicate that, using the total reactivity of the rods with polyethylene in the glory hole, a power in excess of 1,000 watts can be obtained and that about 20,000 watts is the maximum instantaneous power under any circumstances. Although a step input could be arranged in order to reach high powers in less time, a ramp input is sufficient since the temperature does not change significantly during the period when reactivity is added. If the operator can settle the reactor at 1,000 watts, shortly after it achieves this power, the total operating time at this power is estimated from the equation

$$\frac{d(\Delta T)}{dt} = F n_{1000} - \frac{K_o \Delta T}{\rho_o C} \qquad \text{where} \quad \Delta T < \frac{\left(\frac{\rho}{\delta}\right)}{\left(\frac{C_T}{\delta}\right)}$$

Using the data of Section 7 and the temperature when 1,000 watts power is achieved (from Fig. 9) as an initial temperature, the temperature at

which the excess reactivity is overcome is achieved in approximately six minutes. The time is not appreciably increased if a higher conductivity is assigned to the core as the rate of heat generation is significantly greater than the rate of heat flow from the core. With absorbers in the glory hole, the maximum reactivity is less, the temperature when 1,000 watts is achieved is higher, and operating time is reduced as indicated by the behaviour shown in Figure 10.

The calculations indicate that "scramming" the reactor immediately at the end of a high power run (or when power can no longer be maintained) is necessary because of the continued temperature increase that occurs if the reactor is allowed to shut itself down by temperature effects. From the temperature curve of Figure 9, the average temperature increases to 27°C above ambient, and the peak temperature approaches the softening point of the thermal fuse. Scramming the reactor reduces the heat generation rate by a factor of 10 in approximately 13 seconds and by a factor of 100 in approximately 80 seconds; this in turn reduces the temperature buildup considerably.

Three major fields for further research are suggested. First, extensions and refinements of this work would be both informative and interesting, such as extending the analysis to include spatial dependence and determining better estimates of the temperature coefficient, peak power and flux and the temperature distribution. Secondly, there are obvious gaps in the knowledge of nuclear parameters used in this work. In particular, personnel of the various laboratories using polyethylene for critical assemblies need more precise data on its nuclear characteristics. The thermal diffusion coefficient and the Fermi Age in particular are not established. Finally, there is a wide area for research on computer

solutions of the partial differential equations of diffusion and heat transfer problems.

BIBLIOGRAPHY

1. H. Etherington (Editor), Nuclear Engineering Handbook, McGraw-Hill Book Company, Inc., 1958.

2. R. V. Megreblian and D. K. Holmes, Reactor Analysis, McGraw-Hill Book Company, Inc., 1960.

3. W. C. Sangren, Digital Computers and Nuclear Reactor Calculations, John Wiley & Sons, 1960.

4. T. M. Snyder, Proceedings of the International Conference in Geneva, Vol. V pp 162, Aug. 1955.

5. D. J. Hughes and R. B. Schwartz, Neutron Cross Sections (BNL 325) 2nd Edition, 1958.

6. C. H. Westcott, Effective Cross Section Values for Well-Moderated Thermal Reactor Spectra, AECL-1101, Nov. 1960.

7. H. H. Baucom, Jr., Nuclear Data for Reactor Studies, Nucleonics, pp 198, Nov. 1960.

APPENDIX 1

Reactor Kinetic Equations

The equation for the neutron density is

$$\frac{\partial n}{\partial t} = D\nabla^2\phi - \bar{\Sigma}_a\phi + (1-\beta)\nu\varepsilon\bar{\Sigma}_f p P_f \phi + p' P_f' \sum \lambda_i C_i$$

where p' and P_f' are the delayed neutron resonance escape probability and their leakage while slowing down respectively. Assuming a solution may be obtained from the wave equation

$$\nabla^2\phi(\vec{r},t) + B^2\phi(\vec{r},t) = 0$$

$$\frac{dn}{dt} = -\bar{\Sigma}_a\left(1 + \frac{D}{\bar{\Sigma}_a}B^2\right)\phi + (1-\beta)\nu\varepsilon\bar{\Sigma}_f p P_f \phi + p' P_f' \sum \lambda_i C_i$$

Substituting $$L^2 = D/\bar{\Sigma}_a$$

and $$k_\infty\bar{\Sigma}_a = \nu\bar{\Sigma}_f p\varepsilon$$

$$\frac{dn}{dt} = -\bar{\Sigma}_a\left(1+L^2B^2\right)\phi + (1-\beta)k_\infty\bar{\Sigma}_a P_f\phi + p'P_f'\sum\lambda_i C_i$$

Since $\phi = n\upsilon$, $\bar{\Sigma}_a\bar{\upsilon}\left(1+L^2B^2\right) = \frac{1}{\Lambda}$,

$$k_{eff} = \frac{k_\infty P_f}{\left(1+L^2B^2\right)} \quad \text{and} \quad \rho = \frac{k_{eff}-1}{k_{eff}}$$

$$\frac{dn}{dt} = -\frac{n}{\Lambda} + (1-\beta)\frac{k_{eff}}{\Lambda}n + p'P_f'\sum\lambda_i C_i$$

$$= \frac{k_{eff}}{\Lambda}(\rho-\beta)n + p'P_f'\sum\lambda_i C_i$$

When the delayed neutron effectiveness is significantly different from unity, considerations based on importance functions lead to the equation[1]

$$\frac{\partial n}{\partial t} = \left(\frac{k'-1}{\Lambda'}\right)n - \frac{k'\gamma\beta}{\Lambda'}n + \sum\lambda_i C_i \qquad \text{(Eqn 1)}$$

where k' and Λ' are functions of importance and are for a two-group

[1] Reactor Handbook Vol., Physics AECD - 3645, March 1955.

analysis of the steady state:

$$k' = 1$$

$$\Lambda' = \frac{1}{\bar{\Sigma}_a \bar{v}_3 (1+L^2B^2)} + \frac{1}{\bar{\Sigma}_r \bar{v}_4 (1+\tau B^2)}$$

The ratio of k'/Λ' appears in the equation and assuming this is not too different from the k_{eff}/Λ usually considered, the equation is used for reactor solutions.

From the same approach (i.e. weighting the parameter by a factor γ) the equation

$$\rho = \frac{\Lambda}{T k_{eff}} + \gamma \sum \frac{\beta_i}{1+\lambda_i T}$$

is obtained; this equation was used in the experimental reactivity determination. Since the term $\Lambda/T k_{eff}$ was negligible,

$$\frac{\rho}{\gamma} \approx \sum \frac{\beta_i}{1+\lambda_i T}$$

and Eqn 1 can be written as

$$\frac{dn}{dt} = \frac{\gamma k_{eff}}{\Lambda} \left(\left(\frac{\rho}{\gamma}\right) - \beta \right) n + \sum \lambda_i C_i$$

(Eqn 2)

Since the temperature coefficient of reactivity was related experimentally to ρ/γ , the temperature dependent case may be treated with the equation

$$\frac{dn}{dt} = \frac{\gamma k_{eff}}{\Lambda} \left(\left(\frac{\rho}{\gamma}\right) + \frac{C_T}{\gamma} \Delta T - \beta \right) n + \sum \lambda_i C_i$$

(Eqn 3)

Using this notation, the delayed neutron precursor equations have the form

$$\frac{dC_i}{dt} = -\lambda_i C_i + \frac{\gamma k_{eff}}{\Lambda} \beta_i n$$

(Eqn 4)

The temperature depends on the rate of heat generation $\bar{\Sigma}_f \phi e V$

and the rate of heat leakage. Therefore:

$$\frac{d(\Delta T)}{dt} = \frac{\bar{\Sigma}_f n \bar{v} e V}{\rho_o c} - \frac{K_o}{\rho_o c}(\Delta T) \qquad \text{(Eqn 5)}$$

the power at any time may be defined as

$$P = \bar{\Sigma}_f n \bar{v} V \times \left(\frac{1}{3.12 \times 10^{10}} \ \frac{\text{watt-sec}}{\text{fission}} \right)$$

All parameters except ρ may be treated as independent of temperature with small error.

APPENDIX 2

Runga - Kutta Gill Solution of Reactor Kinetic Equations

The equations to be solved are outlined in Appendix 1. For a temperature dependent transient, there are eight simultaneous equations to be solved, for temperature independent cases there are seven.

The program to solve these equations was written in Neliac Compiler language with two tapes required. The second of these contains the data for delayed neutron groups and the operational program. The first tape is made up to the users own requirements. Data which are furnished on the first tape include a program starting address and floating point decimal values for the following in order:

(1) the parameter $\frac{\gamma k}{\Lambda}$ for the reactor in question

(2) the maximum value of reactivity change, positive or negative

(3) the rate of change of reactivity, positive or negative (0 for step input)

(4) the initial average neutron density

(5) the conductance term $\frac{K_o}{\rho_o C}$ (0 for temperature independent case)

(6) temperature coefficient of reactivity

(7) heat generation constant

(8) first time increment for solution (Δt_1)

(9) second time increment for solution (Δt_2)

(10) time increment for print out (Δt_p)

(11) time at which time increments for solutions are to be changed (t_c)

(12) time at which run is to end.

The user must decide where the program is to be located in memory and what parameters to use - then make up a short tape in compiler language as indicated. The second tape remains the same. Two subroutines from the basic library are required, the Runga-Kutta-Gill subroutine (located at 60,200) and "Decof", the floating point output subroutine (located at 71,000). The location of these routines and the compiler location place limits on where the programs may be located, but the compiler can be relocated if necessary.

In operation, the program dumps on magnetic tape the values fed in on the first tape for reference purposes, then computes initial values for temperature and the delayed neutron percursors, establishes the conditions for a Runga Kutta Gill solution and, based on whether $\frac{K_o}{\rho_o c}$ is zero or has a value, selects the routine for a temperature independent or a temperature dependent problem. Until time t_c, it uses the time increment Δt_1, then changes to use the time increment Δt_2. This feature was included such that a shorter time increment for the first few seconds of a step input problem could be used. After each time increment $2 \times \Delta t_p$ four or six values are dumped on magnetic tape. For the temperature independent case, two consecutive times (in seconds) and the corresponding neutron densities are dumped, for the temperature dependent case, the temperature at each time is also dumped.

APPENDIX 3

A Two-Group, Two-Region Computer Program with Cylindrical Geometry

For each region and group, the neutron behaviour in steady state conditions is defined by equation of the form

$$D\nabla^2 \phi_i(r,z) - \Sigma \phi_i(r,z) + S_o(r,z) = 0$$

where the coefficients are assumed constant throughout the region, and the equations in a region are coupled through the source terms $S_o(r,z)$ where 'o" signifies "other group".

These equations may be replaced by finite difference equations of the form (3)

$$a_{n,m}\phi_{n,m+1} + b_{n,m}\phi_{n,m-1} + c_{n,m}\phi_{n+1,m} + d_{n,m}\phi_{n-1,m} - s_{n,m}\phi_{n,m} + e_{n,m} = 0$$

where the coefficients are functions of position, mesh spacing and the coefficients of the partial differential equations.

For the reactor problem, a core diameter and height of 12.5 cm was selected with an extrapolated diameter and height for the shielding of 42.5 cm. These dimensions where chosen to allow one centimetre spacing with zero mesh points on the outside boundaries and on the core-reflector interface. Due to symmetry, only 1/4 of the configuration is required. The total mesh consists of 44 rows and 44 columns with 1936 mesh points.

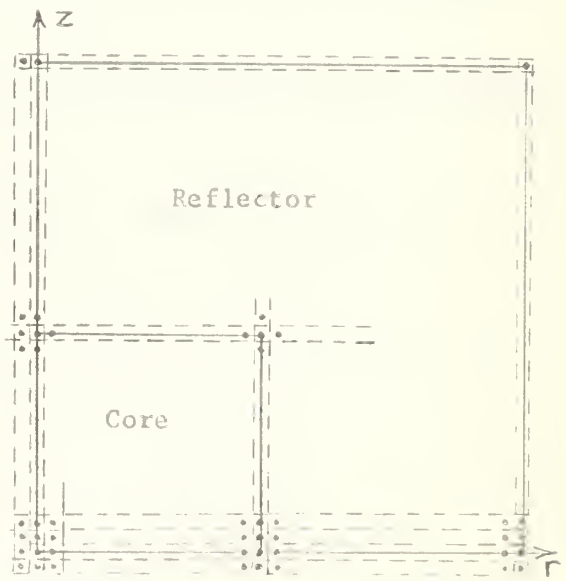

Row 44 and column 44 along the exterior boundaries have zero values, row 1 and column 1 beside interior boundaries have mirror

image values across the axis.

The method of solution used was the alternating-direction technique outlined by Peaceman & Rackford.[1] In this method, all the rows are selected in turn and solved by the Gaussian elimination technique for linear equations with a coefficient matrix of triple diagonal form. The procedure is repeated for the columns in turn. Solving the rows and columns once constitutes one pass of the routine. During the solution for any one row or column, the values in the adjacent row or column respectively are assumed known such that the five point difference equation has the form

$$a_{n,m}\phi_{n,m+1} + b_{n,m}\phi_{n,m-1} - \mathcal{C}_{n,m}\phi_{nm} = -c_{n,m}\phi_{n+1,m} - d_{n,m}\phi_{n-1,m} + \mathcal{D}_{n,m}\phi_{n,m} - e_{nm}$$

where "m" signifies the row (or column) which is to be solved. $\mathcal{C}_{n,m}$ and $\mathcal{D}_{n,m}$ are functions of the coefficients $a_{n,m}$, $b_{n,m}$, $c_{n,m}$ and $d_{n,m}$ and an iteration parameter which is varied depending on which pass is being executed (the parameter is large for initial passes, lower as the number of passes increases).

The program for this problem was written in Neliac Compiler language and consisted of

(1) Storage areas for coefficients, computed data and intermediate data.

(2) Routine for calculating all of the coefficients a_{nm}, b_{nm}, etc., and storing for future use.

(3) A Peaceman-Rackford method subroutine, entered from the main program.

[1] D. W. Peaceman and H. H. Rachford, Jr., "The Numerical Solution of Parabolic and Elliptic Differential Equations", J. Soc. Indust. Appl. Math., 3(1955), p. 28.

(4) An "Equation" subroutine to solve a row or column, entered from the Peaceman-Rackford method subroutine.

(5) Main program, which alternately selected computation of fast group and slow group, provided checks and dumped computer data.

Such a program would not be expected to be short due to the storage and extensive transfer requirements. Approximately 12,000 cells were required for storage and a further 2,200 for routines of which most were required for the coefficient calculation and the Peaceman - Rackford method subroutine. One more versed with computer programming could reduce these requirements considerably. What was lost in the space sense was gained in time by having many coefficients in storage "on call" rather than calculating them as required. A complete pass through the Peaceman - Rackford method routine, which involves calculation and transfer on two blocks of 1,939 values each using the equation subroutine, required about 4 seconds.

In operation, convergence difficulties were encountered which could not be eliminated by extensive "de - bugging" and may indicate the necessity of a new approach.